LASER INTERFEROMETER GRAVITATIONAL WAVE OBSERVATORY
- LIGO -
CALIFORNIA INSTITUTE OF TECHNOLOGY
MASSACHUSETTS INSTITUTE OF TECHNOLOGY

Technical Note	LIGO-T1900380–v1	31st October 2019

2-micron, HIGH QE Photodetector for Quantum Metrology

Shalika Singh
Mentors: Dr Koji Arai, Rana X. Adhikari, Duo Tao

California Institute of Technology
LIGO Project, MS 18-34
Pasadena, CA 91125
Phone (626) 395-2129
Fax (626) 304-9834
E-mail: info@ligo.caltech.edu

Massachusetts Institute of Technology
LIGO Project, Room NW22-295
Cambridge, MA 02139
Phone (617) 253-4824
Fax (617) 253-7014
E-mail: info@ligo.mit.edu

LIGO Hanford Observatory
Route 10, Mile Marker 2
Richland, WA 99352
Phone (509) 372-8106
Fax (509) 372-8137
E-mail: info@ligo.caltech.edu

LIGO Livingston Observatory
19100 LIGO Lane
Livingston, LA 70754
Phone (225) 686-3100
Fax (225) 686-7189
E-mail: info@ligo.caltech.edu

http://www.ligo.caltech.edu/

Contents

1 Introduction and Context **2**

2 Objectives **2**

3 Experiment overview and approach **3**

3.1 Overview 3

3.2 Detailed Explanation of Procedure 4

4 Characteristics of photodiodes studied **6**

4.1 Quantum Efficiency (Q.E.) 6

4.2 Noise Measurement of photodiode 8

5 Experimental Work **10**

5.1 Overview of Circuit 10

5.2 Transimpedance Amplifier(TIA) 12

5.3 Differential Circuit 18

5.4 Whitening Filter 20

5.5 Sallen-Key Filter 22

5.6 Voltage Regulator 24

5.7 Dark Current Measurement of Photodiodes 25

5.8 Dark Noise Measurement of Photodiodes 31

5.9 1/f noise Measurement of Photodiodes 36

5.10 Quantum Efficiency(Q.E.) Measurement of Photodiodes 38

6 Conclusion **41**

7 Future Work **41**

1 Introduction and Context

The Advanced LIGO detectors are the second generation of interferometers designed with increased sensitivity to GW strain. It almost provides a factor of 10 increase in strain sensitivity over a broad frequency band. The basis of the optical configuration of the Advanced LIGO interferometer is a Michelson interferometer with a Fabry-Perot resonant cavity in each arm. This builds up the phase shift produced by an arm length change. The arm lengths need to be controlled with high precision to keep the light resonating in arm cavities. This problem involves five degrees of freedom namely, the arm cavity lengths, the differential and common mode lengths of the interferometer and the wavelength of the laser.

The Advanced LIGO interferometer is the most sensitive instrument and Voyager is being planned as an upgrade to it. Voyager will use a 2um laser instead of the present 1064nm laser. Shifting to 2um will be advantageous as it will lower the noise of GW detectors but it will involve new range of technologies. New material for the photo-detectors is an important requirement. We desire to have photodiodes with quantum efficiency of greater than 99 percent and low noise, which is very important for quantum noise reduction with squeezed vacuum injection. The InGaAs photodiodes that are currently being used are not sensitive to 2μm wavelength of laser so we need different material of photodiode. Another important change will be the mirrors, or test masses, that provide the signal from passing GWs. The new test mass will be of 200-kg and made of pure crystalline silicon with amorphous-silicon coatings. The absorption level of the silicon coatings will drop off dramatically near 2um. It will help us to operate at high power levels without worrying about thermal problems. Additionally, the temperature of the test masses will be lowered to 123K for substantial decrease in noise.

2 Objectives

The prime goal of this project was to characterize various types of photodiodes that are sensitive to 2μm wavelength of incident laser power. The wavelength of laser to be used is 2μm, which is the same as the wavelength of the laser to be deployed in Voyager. The characterization included measurement of the external and internal quantum efficiency, dark current, dark noise and flicker noise of the photodiodes at room temperature.

3 Experiment overview and approach

3.1 Overview

This experiment involved characterization of photodiodes(PD) at room temperature using a very low noise electronics circuit. The photodiodes under test are the extended InGaAs photodiodes from Laser Components(IG22X2000T9) and InAsSb photodiode from NASA JPL. These photodiodes are sensitive at 2μm. We measured the external and internal quantum efficiency, dark current, dark noise and flicker noise of these photodiodes.

The energy of photon from a 2μm laser is 0.62 eV. Hence, the material of photodiodes are chosen in such a way that the bandgap is less than the energy of incident photon. So, electrons can easily start conducting by moving an electron (generated from electron hole pair), to conduction band from the valence band. The band gap shouldn't be very small, else the photodiode will start conducting at room temperature as electrons will be easily excited, hence will add to the noise.

The JPL Indium Arsenide Antimonide, InAsSb PD had three PD on one surface. They were of area $(500\mu\text{m})^2$, $(750\mu\text{m})^2$ and $(1000\mu\text{m})^2$.

The Extended Indium Gallium Arsenide, ex-InGaAs PD were two in number. They had a diameter of 2mm. The two PD were named as X8905 and X8906 respectively. The responsivity of ex-InGaAs is 1.3 A/W.

JPL InAsSb
Sb3513_A2

Extended InGaAs
IG22X2000T9

Figure 1: Photodiodes

3.2 Detailed Explanation of Procedure

The photodiodes were tested at room temperature. The photodiode(PD) was inserted in a socket and the pins of the socket were used to make any type of connections to the PD. The laser was projected using the fibre launcher and was properly focused using converging lens of appropriate focal length. A switchable breakout box was used with had a receiving point for connections from the PD. The breakout box was used to apply the bias to the appropriate pin of the respective PD. It was also used to receive the output from the photodiode. The BNC connectors were used to make further connections from the breakout box.

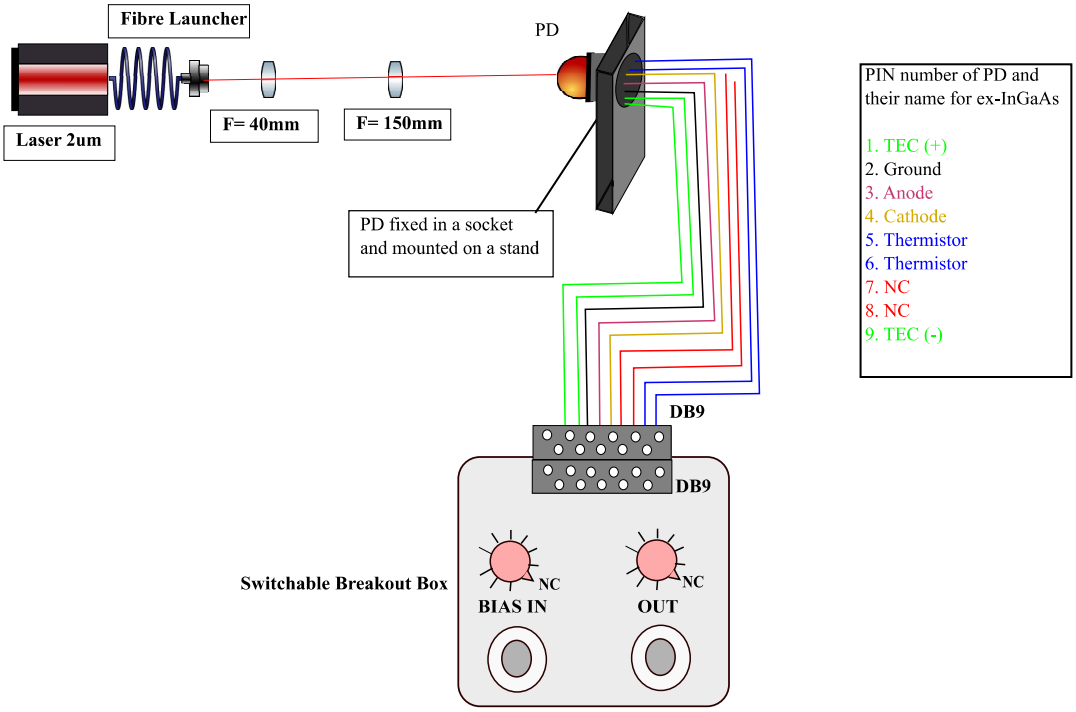

Figure 2: Representation of Experimental Setup

The circuit box comprised of a generic prototype board containing a Sallen key filter, transimpedance amplifier, differential circuit, whitening filter and voltage regulators. The voltage regulator made the 15V supply clean and the circuit was free of any undesirable noise. The transimpedance amplifier was used to convert the current output of photodiode to voltage and also to amplify it. The differentiating circuit will help us to measure the relative shot noise of the photodiode. A Whitening filter will help us in smoothing all the frequency contents to a constant power spectral density. The walls of the box were fixed with the BNC connectors to make connections to and from the box.

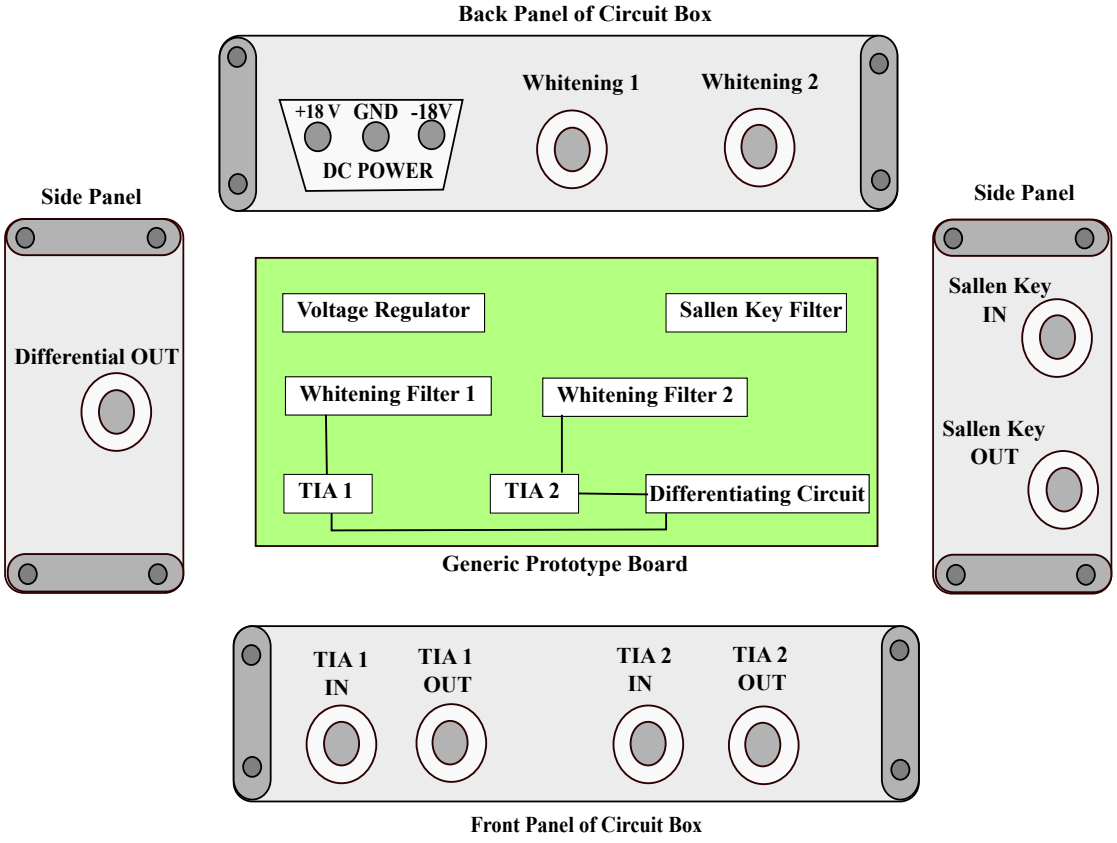

Figure 3: Circuit Box

4 Characteristics of photodiodes studied

4.1 Quantum Efficiency (Q.E.)

LIGO requirements call for a net quantum efficiency of 99% from the beam splitter to the detection electronics.

4.1.1 External quantum efficiency

The external quantum efficiency can be measured using a power meter and a laser source incident on the photo-diode. The external quantum efficiency, E.Q.E. of any photodiode is defined as the fraction of incident photons that contribute to the photocurrent.

$$E.Q.E. = \left(\frac{R_\lambda}{0.858[\mathrm{A/W}]}\right) \cdot \left(\frac{1064[\mathrm{nm}]}{\lambda}\right) \tag{1}$$

$$R_\lambda = \frac{I}{P} \tag{2}$$

where $\mathrm{h} = 6\,63 \times 10^{-34}\mathrm{Js}$, is the Planck constant, $\mathrm{c} = 3 \times 10^{8}\mathrm{m/s}$, is the speed of light, $\mathrm{q} = 1\,6 \times 10^{-19}\mathrm{C}$, is the electron charge, R_λ is the responsivity (ratio of incident photo-current I, to the incident light power P at a given wavelength) in A/W and λ is the wavelength of light in nm.

4.1.2 Internal Quantum Efficiency

When the laser of power $\mathrm{P_{in}}$, is incident on the photodiode, there is some amount of power that is reflected from the surface of the PD, $\mathrm{R_{refl}}$. The internal quantum efficiency, I.Q.E. can be calculated by subtracting the amount of power reflected from the external quantum efficiency, E.Q.E.

Then the reflectivity, R is given by;

$$R = \frac{\mathrm{R_{refl}}}{\mathrm{P_{in}}} \tag{3}$$

and the I.Q.E is given by;

$$I.Q.E. = \frac{E.Q.E.}{1 - R} \tag{4}$$

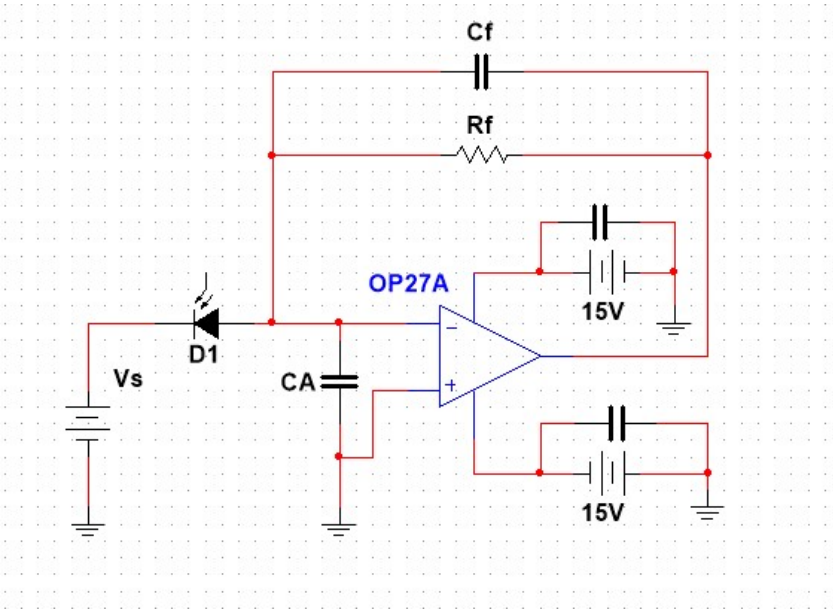

Figure 4: Circuit setup of Photo-diode and TIA

The PD is used in series with a transimpedance amplifier, which converts the current to voltage and also amplifies it according to the gain of the TIA. The corresponding photodiode can be reverse biased and additionally connected to an OpAmp with a resistor in feedback loop. In order to keep minimum errors, the bias voltage must be very clean; meaning low noise and good temperature stability. The dark current will be directly proportional to the bias voltage applied to the PD.

4.2 Noise Measurement of photodiode

The noise floor for this system is determined by noise features of the photodiodes, quantum noise and thermal noise.

Several sources are responsible for the photodiode noise, mainly, dark noise, shot noise, flicker noise $1/f$ noise) and generation-recombination (G-R) noise. Material properties of the various electronic components used, will contribute to the thermal noise of the system.

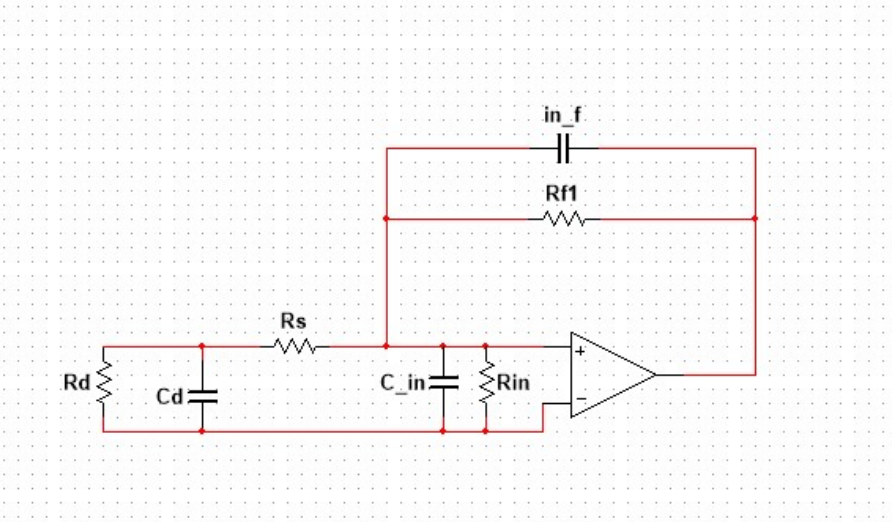

Figure 5: The Equivalent noise circuit for a photodiode in series with TIA

The photodiode is represented as a current source, with capacitor Cd in series with resistance Rs. The total noise of the PD will be the sum of all its components.

4.2.1 Shot noise

A fundamental limit to the optical intensity noise is given by the shot noise. The fluctuations in the flux of the electron and hole currents that carry the electrical current, result in the shot noise. The shot noise current for a reverse biased photodiode is,

$$(\mathrm{i_{shot}}) = \sqrt{2\,q\,I_d\,\Delta f} \tag{5}$$

Where, q is the electron charge, I_d is the photodiode current, and Δf is the noise equivalent bandwidth (NEB).

The balanced homodyne detector configuration can be used for measurement. We will be using two photo-diodes and the beam splitter will be sending 50% of power to one photo-diode and the remaining 50% to another. A differential circuit can be used to provide the reference of the shot noise level.

4.2.2 Dark Current

Even in the absence of any optical power on the photodiode it can produce a small amount of signal current, which is called dark current. Defect states related to crystals or impurities can cause thermal excitation of carriers. It can also occur due to the thermionic emission on the photocathode. Since it's temperature dependent low temperature operation are favorable. We can use measure the dark current in the same way as photocurrent but with laser power switched off.

4.2.3 Dark noise

Photodiode dark noise arises due to dark current which varies directly with temperature in photoconductive mode.

4.2.4 Flicker noise

The noise at low frequency may be contributed from two sources. One is the flicker noise that dominates at low frequencies. It is one of the main limiting factors in detection sensitivity. The current spectral density of the flicker noise can be evaluated using the semiempirical expression:

$$S_{i,1/f} = \frac{I_{dark}^{\beta} k}{f^{\gamma}} \tag{6}$$

where, I_{dark} is the PD dark current, k and γ are the coefficients of the photodiode that depend on fabrication process like quality and technology, β value is an empirical constant that depends on the doping, and f is the frequency.

4.2.5 Generation-Recombination noise

Another noise component that is contributed by low frequency is the generation recombination (G-R) noise. The fluctuations in the carrier flux due to generation, recombination, and trapping of carriers in semiconductors are manifested as noise due to variation in the number of free carriers. The spectral response of G-R noise is almost uniform up to a frequency which is determined by the lifetime of the carriers in the photo-detectors.

4.2.6 Total noise of photodiode

The photodiode noise can be approximated by the following expression, which takes into account the 1/f noise, shot noise and generation recombination noise,

$$i_{\mathrm{Pd}} = i_{1/f} + i_{\mathrm{shot}} + i_{\mathrm{gr}} \tag{7}$$

5 Experimental Work

5.1 Overview of Circuit

The photodiode is to be used in photoconductive mode, hence a reverse biased voltage of upto 1V. The resulting photocurrent is linearly dependent on the incident laser power. The magnitude of reverse voltage has minimal influence on the photocurrent. The TIA converts current to voltage. The TIA is connected to whitening Filter for any amplification, if needed. We have two TIA for two photodiodes. The output of the two TIA are connected to a differential circuit, in order to study the shot noise of the photodiode.

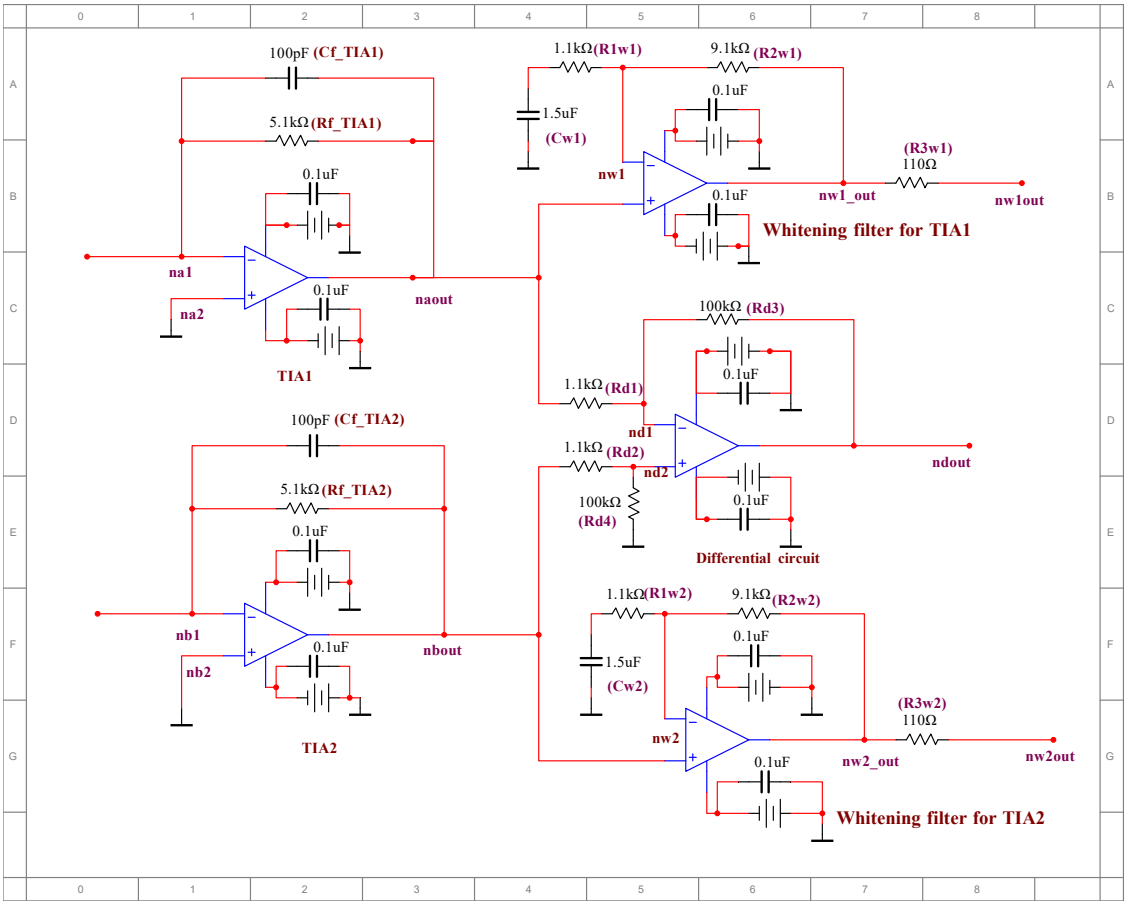

Figure 6: Complete Circuit Diagram

The circuit was made onto a generic prototype board and put in a box with BNC connectors.

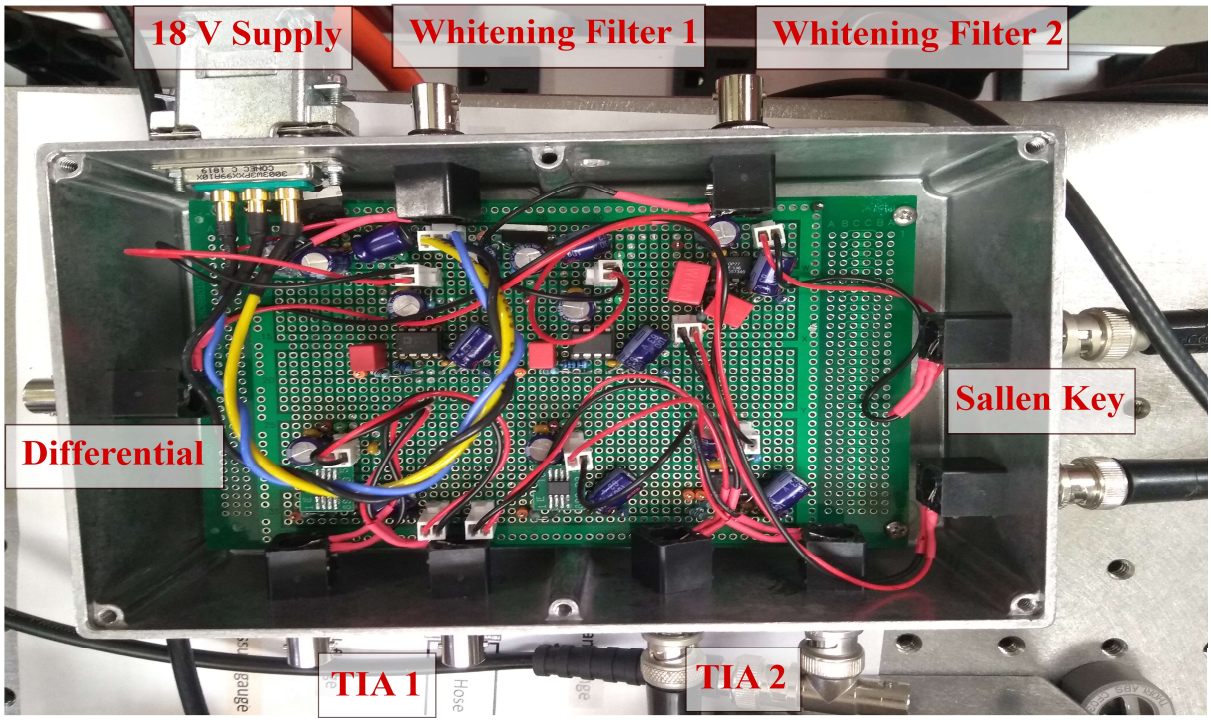

Figure 7: Circuit in a Box

5.2 Transimpedance Amplifier(TIA)

The power incident on a photodiode produces a photocurrrent, a TIA is used to convert the current to voltage and also amplify it by using an appropriate design. In order to measure the dark current and photocurrent, the TIA was designed in such a way that its noise does not mask the measurements from the photodiode.

We designed a TIA with a gain of 5.1k and compared the noise by using different Operational Amplifiers. We used OP27, LT1792, LT1012, OPA140, AD820. The noise of TIA was analyzed using the SR785 spectrum analyzer and also compared with results of simulation using ZERO. The input referred noise was obtained by dividing the noise at output by the transfer function of the TIA.

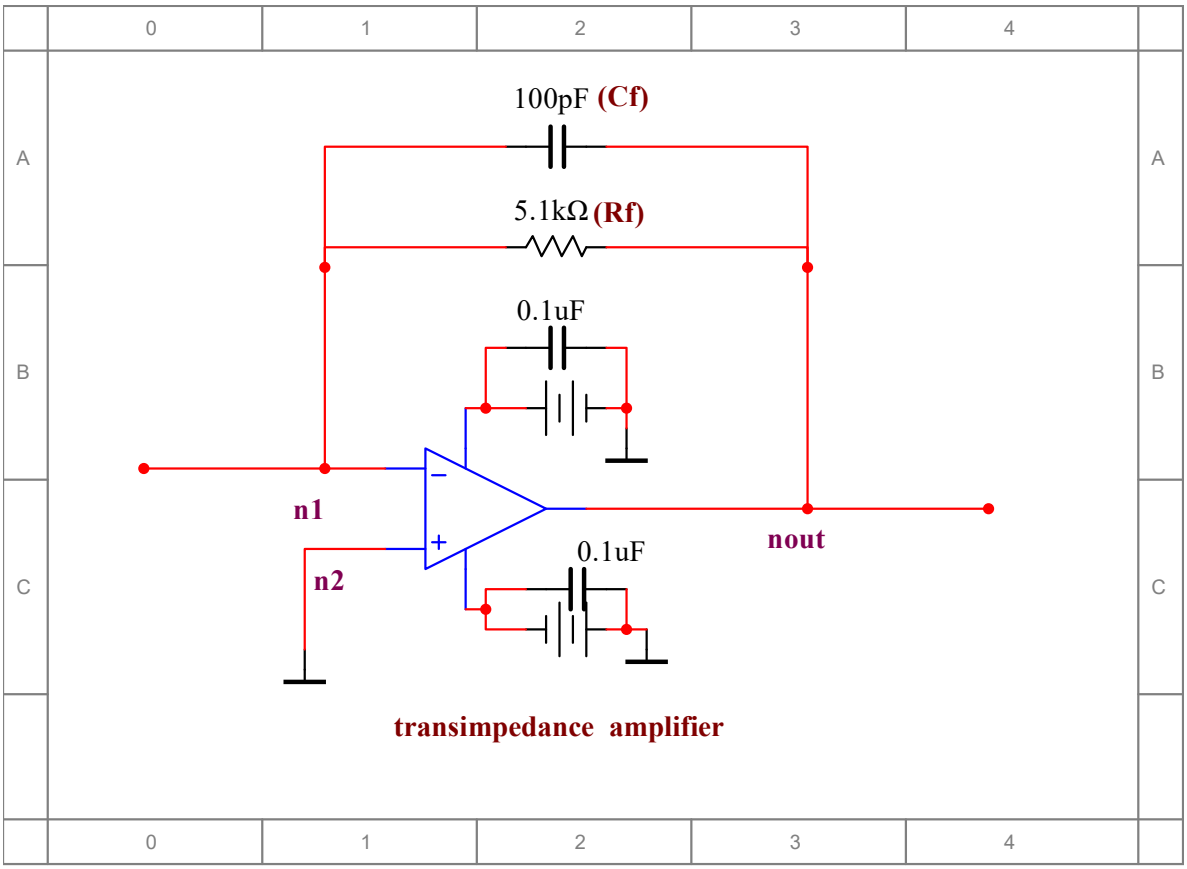

Figure 8: Design of transimpedance amplifier

5.1.2 Noise Comparison Between Different OpAmps

The noise across transimpedance amplifier was obtained for different OpAmps and compared. It was observed the TIA has least noise when designed using OPA140. Te noise of OPA140 was observed to be around be 8 pA/$\sqrt{\text{Hz}}$ at 10 Hz and 4 pA/$\sqrt{\text{Hz}}$ above 100Hz.

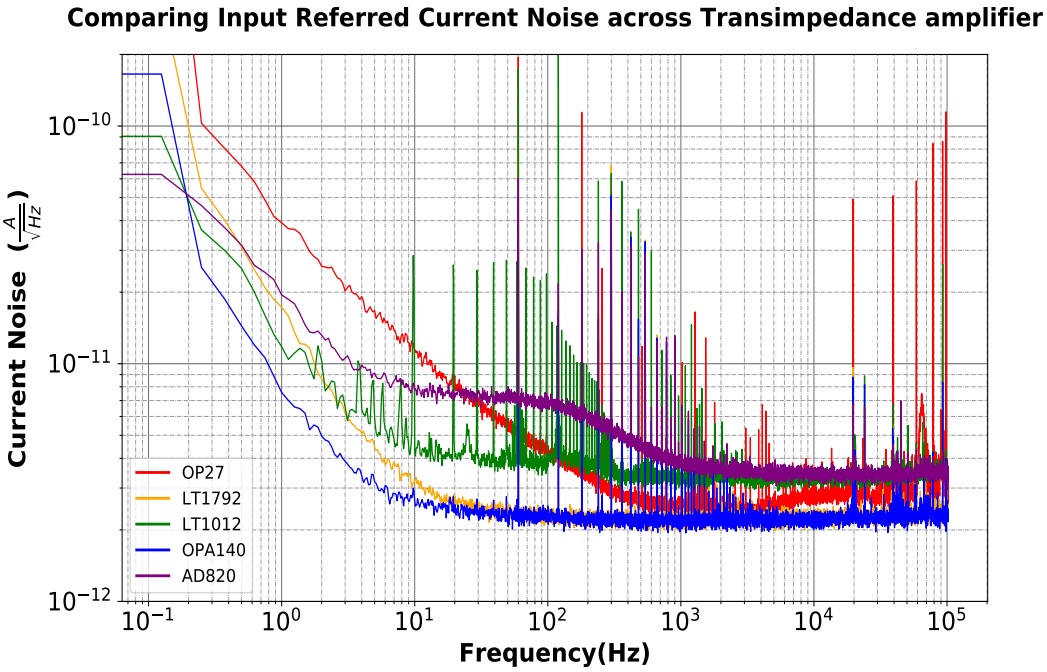

Figure 9: Noise Comparison of TIA using different OpAmps

The Noise of TIA using OPA140 is comparable to shot noise produced from a DC current of 1mA(considering a bandwidth of 0.02 Hz, which is 2 pA/$\sqrt{\text{Hz}}$. So we finally chose the TIA made using OPA140 for this experiment.

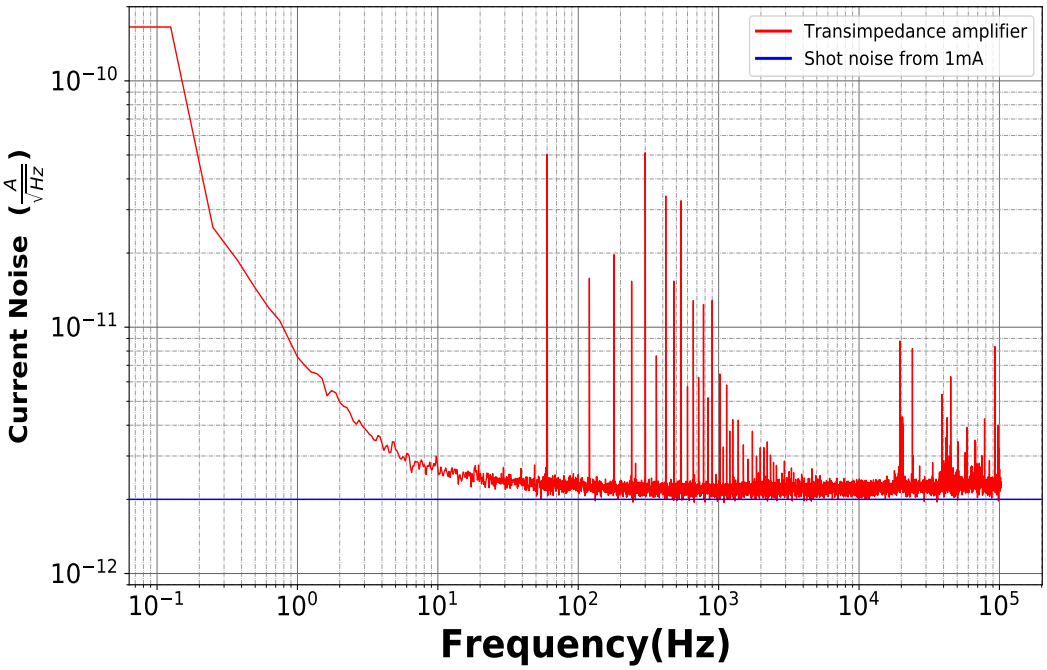

Figure 10: Low noise electronics

5.1.2 TIA using OP27 OpAmp

The input referred current noise was observed to be 10 pA/$\sqrt{\text{Hz}}$ at 10Hz and 3 pA/$\sqrt{\text{Hz}}$ above 1 kHz. There is a difference of 1 pA/$\sqrt{\text{Hz}}$ between the experimental results and simulated results, above 100Hz.

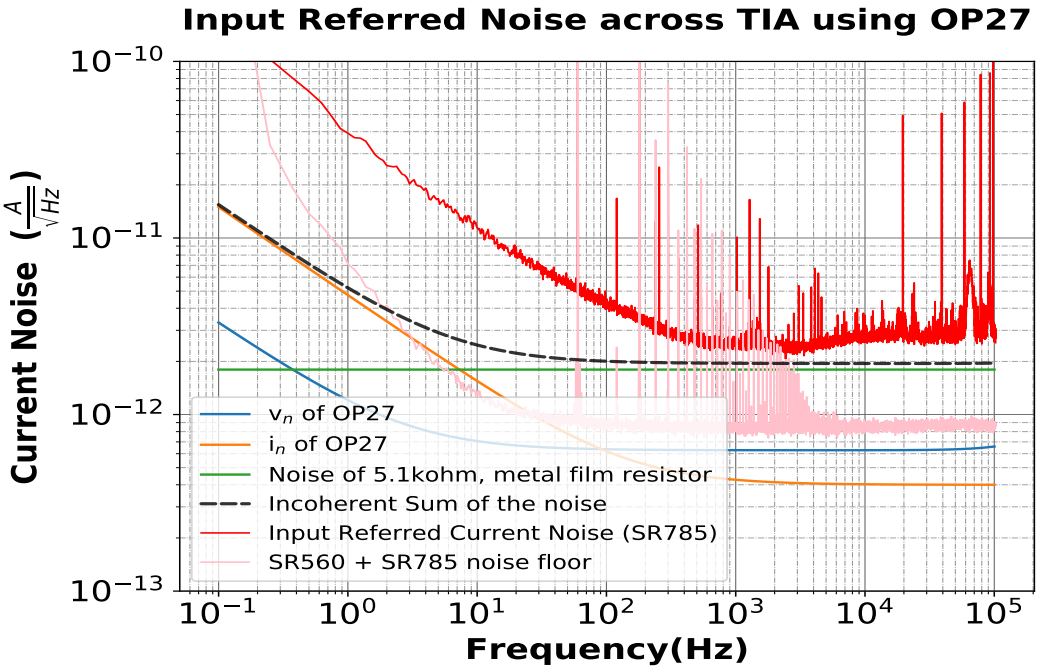

Figure 11: Noise across TIA using OP27

5.1.3 TIA using LT1792 OpAmp

The input referred current noise was observed to be 3 pA/$\sqrt{\text{Hz}}$ at 10 Hz and 2 pA/$\sqrt{\text{Hz}}$ above 100 Hz. The simulated and experimental results match to a great extent above 100 Hz. The noise here is mainly dominated by the Johnson noise of the 5.1$k\Omega$ resistor.

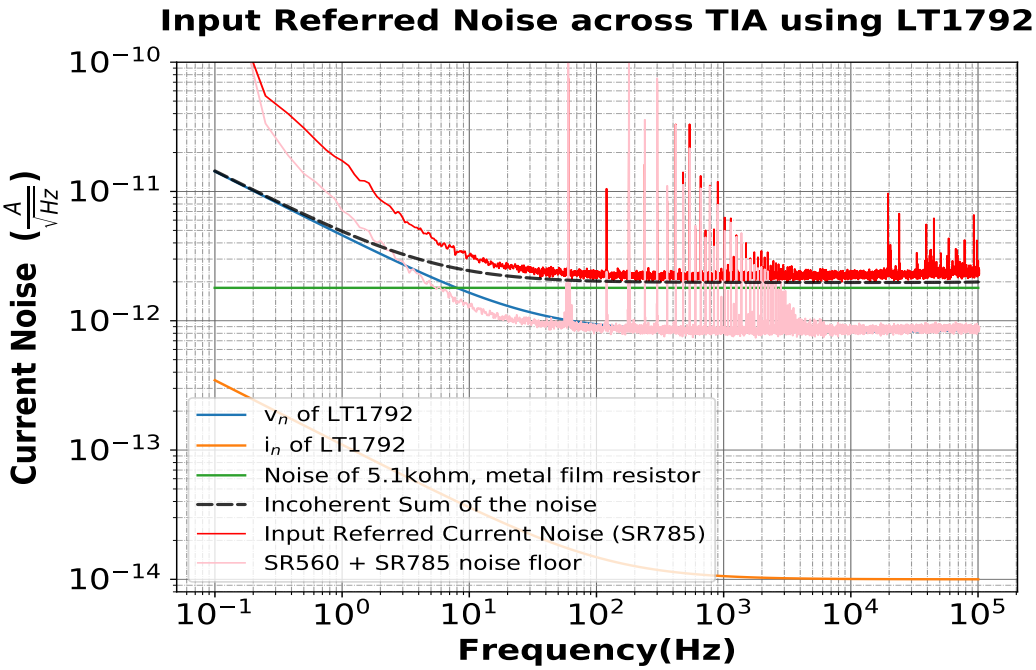

Figure 12: Noise across TIA using LT1792

5.1.4 TIA using LT1012 OpAmp

The input referred current noise was observed to be 4 pA/$\sqrt{\text{Hz}}$ at 10 Hz and 3 pA/$\sqrt{\text{Hz}}$ above 100 Hz. The simulated results and experimental results match to a great extent above 10Hz. The noise in this case is mostly dominated by the noise of the OpAmp LT1012 itself.

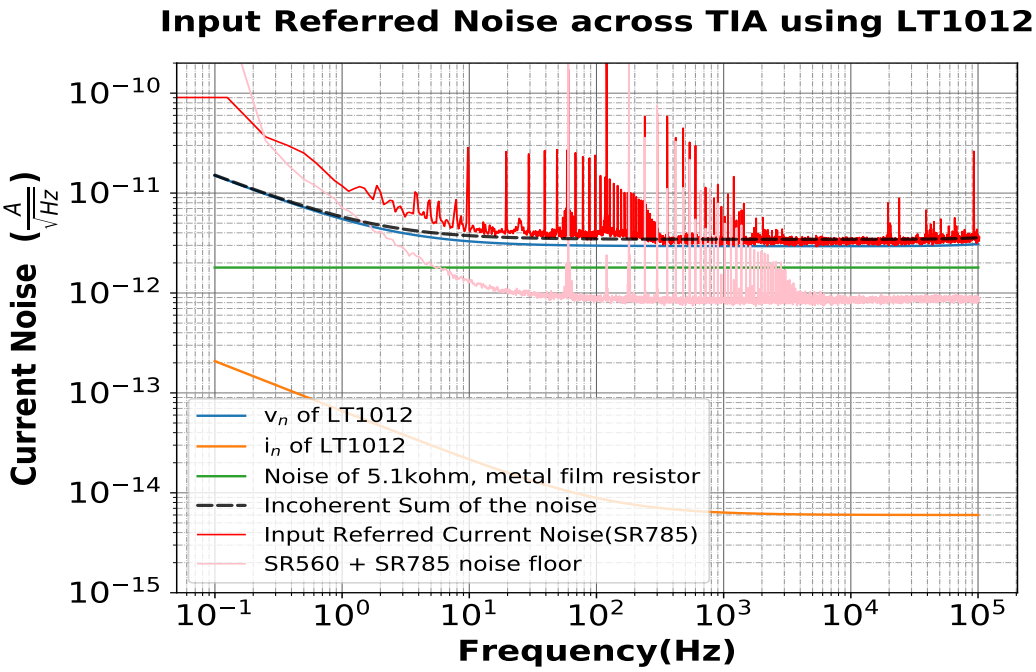

Figure 13: Noise across TIA using LT1012

5.1.5 TIA using OPA140 OpAmp

The input referred current noise was observed to be 3 pA/$\sqrt{\text{Hz}}$ at 10 Hz and 2 pA/$\sqrt{\text{Hz}}$ above 30Hz. The simulated results and experimental results match to a great extent above 10Hz.The noise in this case is mostly dominated by the Johnson noise of the 5.1$k\Omega$ resistor.

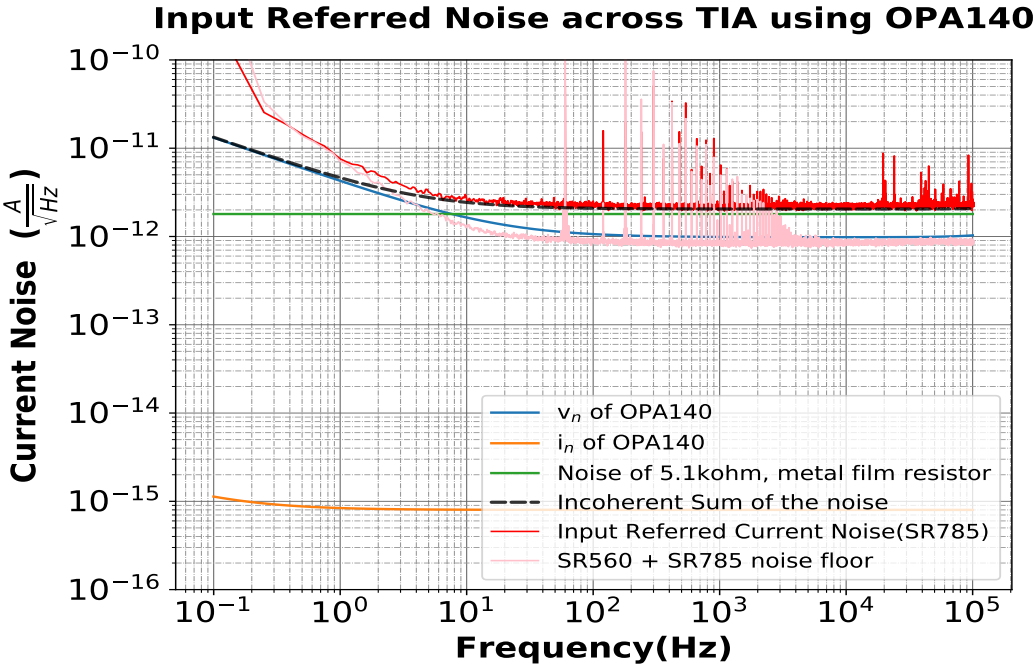

Figure 14: Noise across TIA using OPA140

5.1.6 TIA using AD820 OpAmp

The input referred current noise was observed to be 8 pA/$\sqrt{\text{Hz}}$ at 10 Hz and 4 pA/$\sqrt{\text{Hz}}$ above 100Hz. The simulated results and experimental results match to a great extent below 10Hz and above 100Hz. The noise in this case is mostly dominated by the noise of AD820 itself.

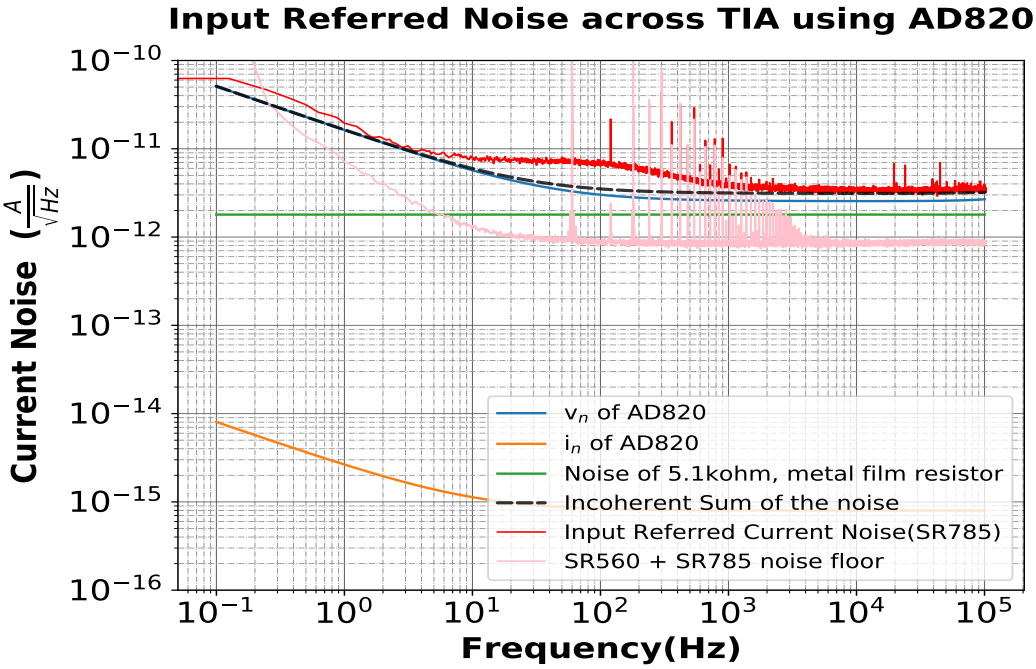

Figure 15: Noise across TIA on using AD820

5.3 Differential Circuit

A differential amplifier circuit amplifies the difference between two input voltages but suppresses any voltage common to the two inputs. The differential circuit was designed to know the shot noise of the photodiode using balanced homodyne detection. The calculation of shot noise is one of the future goals of this experiment. The photocurrent can be converted into voltage using TIA and the outputs of two TIA can be fed as input to this differential circuit and hence know the shot noise of the photodiode.

We made the differential circuit using an OP27 and it has a gain of 90.9.

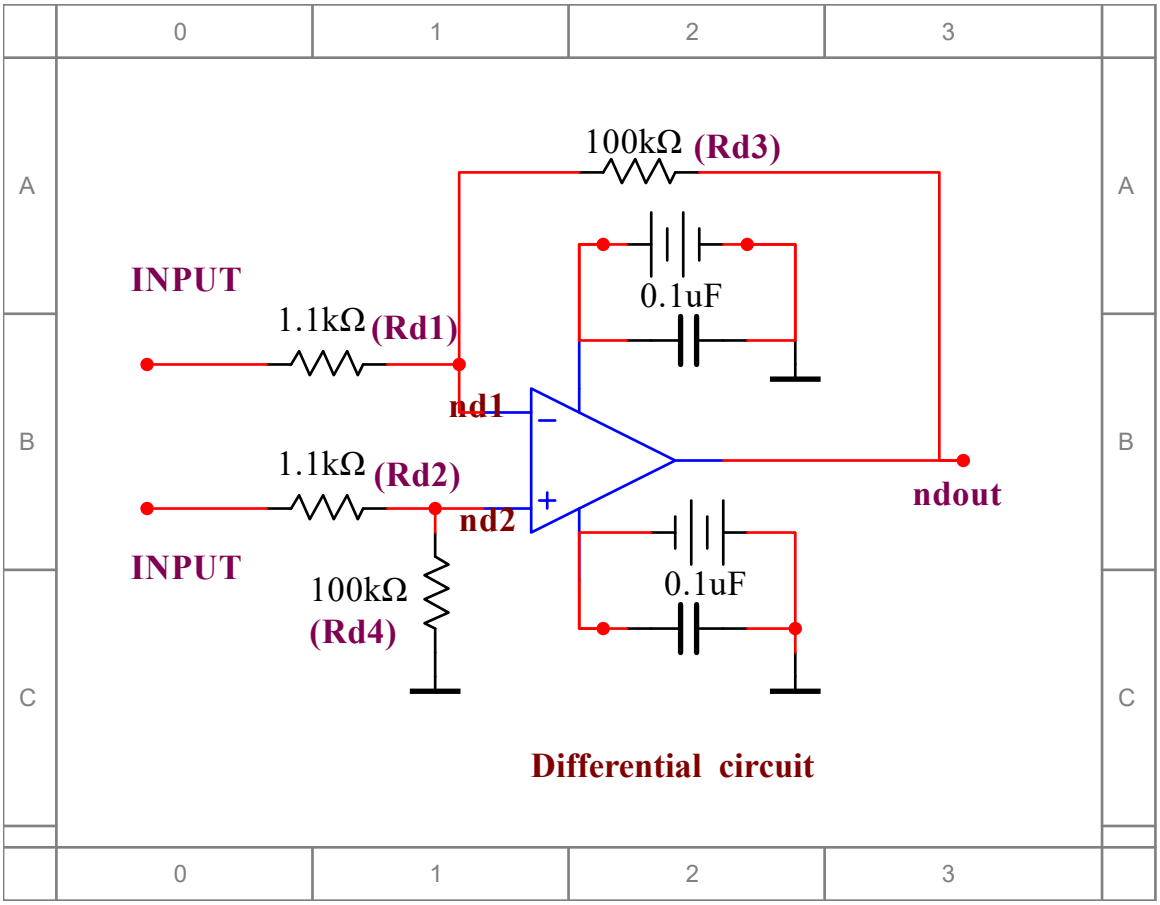

Figure 16: Differential Circuit

The noise level of the differential circuit was measured by shorting both the input terminals and observing the output at the pin6 of IC. The noise level was then divided by the transfer function to project the noise at the input. The input referred voltage noise was observed to be 20 nV/$\sqrt{\text{Hz}}$ above 10 Hz.

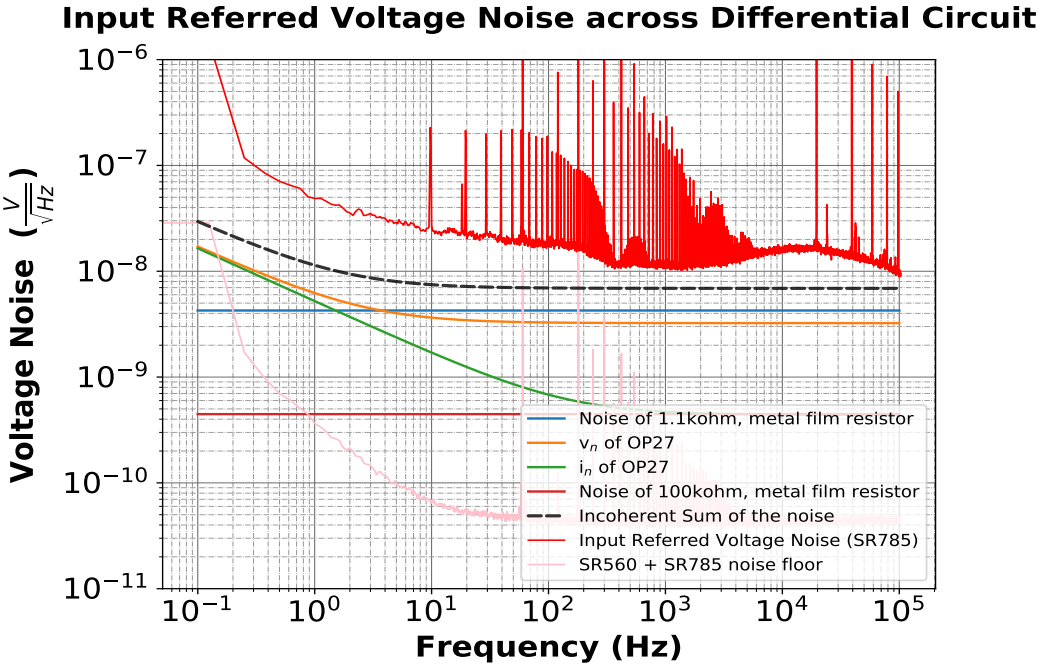

Figure 17: Differential Circuit Noise

5.4 Whitening Filter

The whitening filter is used to remove as much correlation as possible from the residual. This can be used in combination with the TIA. We designed a whitening filter having cut off frequencies at 10 Hz and 100 Hz. This filter was made using OP27 and the filter had a gain of 10.

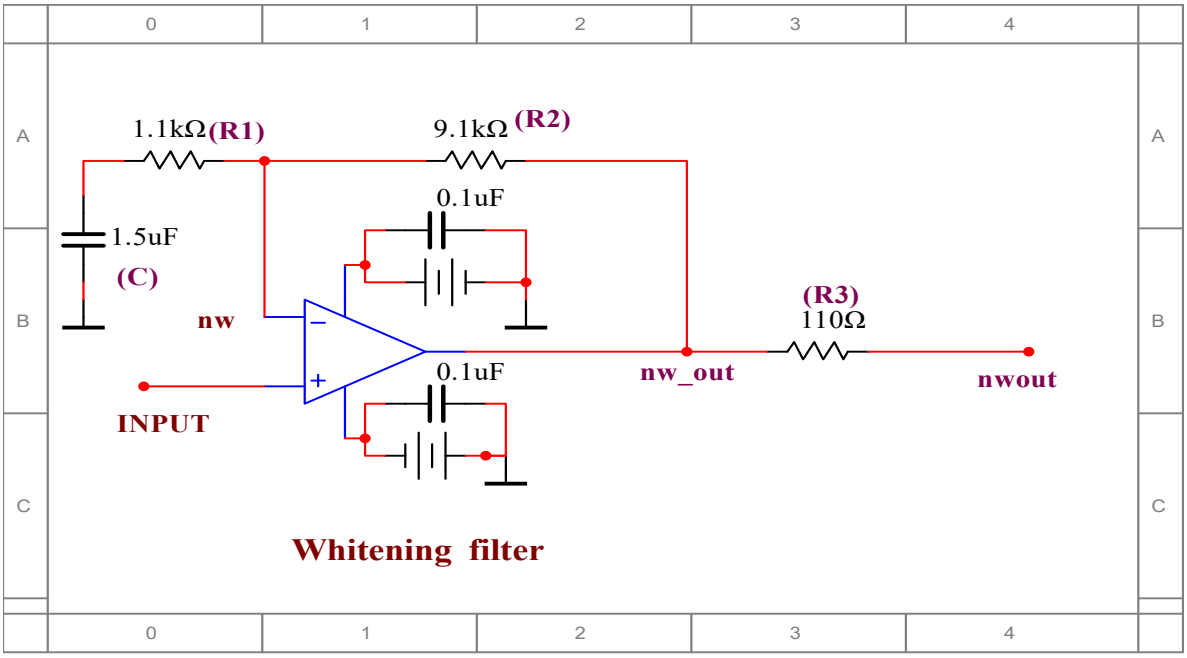

Figure 18: Whitening Filter

The selection of resistors and capacitor was done by using the calculations as shown below.

$$G = 1 + \frac{R_2}{Z_1} \tag{8}$$

$$Z1 = \left(\frac{1}{R_1} + \mathrm{i}\,\omega\, C\right)^{-1} \tag{9}$$

Now since the cut off frequencies were 10 Hz and 100 Hz with a gain of 10. We assumed zero frequency, f1 = 10Hz and pole frequency, f2 = 100Hz.

$$G = \frac{1 + \frac{f}{f1}}{1 + \frac{f}{f2}} \tag{10}$$

For the particular design,

$$G = 1 + \frac{R_2\,\mathrm{i}\,\omega\,C}{1 + \mathrm{i}\,\omega\,C\,R_1} \tag{11}$$

Replacing $\mathrm{i}\,\omega$ with s, the above equation can be transformed as,

$$G = \frac{1 + s\,C\,(R_1 + R_2)}{1 + s\,C\,R_1} \tag{12}$$

Therefore from above equation we can find the values of resistors as

$$f1 = \frac{1}{C\,(R_1 + R_2)\,2\pi} \tag{13}$$

$$f2 = \frac{1}{C\,R_1\,2\pi} \tag{14}$$

Taking $C = 1.5\mu$F, we get $R_1 = 1.1$kΩ and $R_2 = 9.1$kΩ.

The noise of the Whitening filter was measured by grounding the input terminal (pin 3) and taking the measurement at the output. The input referred voltage noise is 5 nV/$\sqrt{\text{Hz}}$ above 100 Hz.

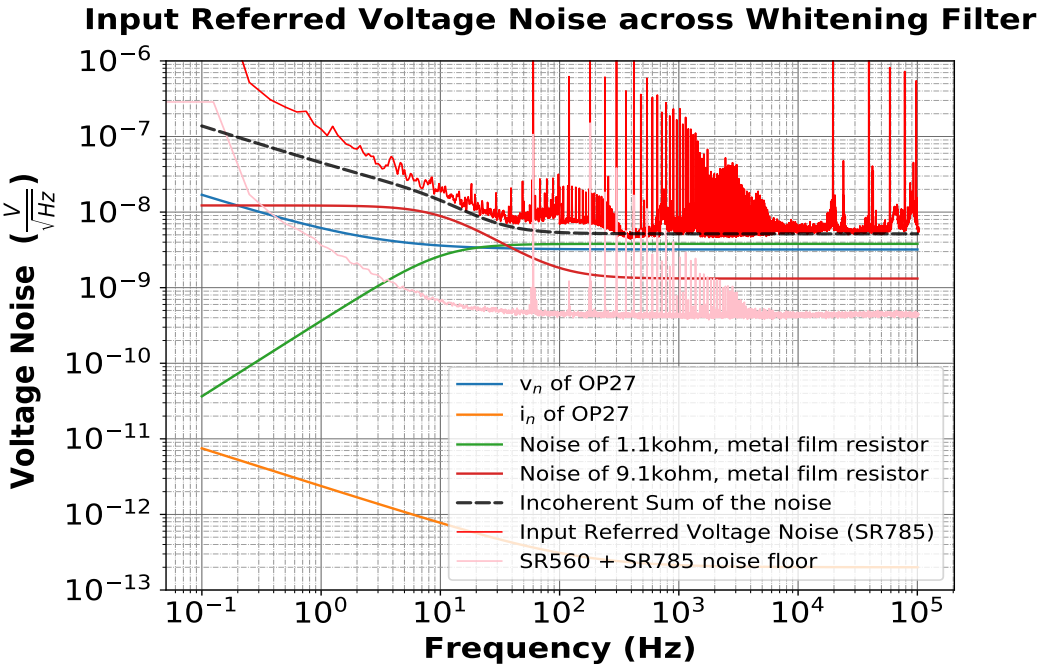

Figure 19: Whitening Filter noise

5.5 Sallen-Key Filter

The Sallen-Key filter is a second order filter. The design is based around a single non-inverting operational amplifier and two resistors. This creates a voltage-controlled voltage source design with filter characteristics of, high input impedance and low output impedance and good stability. In our case we needed to provide a bias of 1V to the photodiodes so we designed a low pass Sallen-Key filter with a cut-off frequency of 1 Hz and unity gain. We used OP27 as the non-inverting OpAmp.

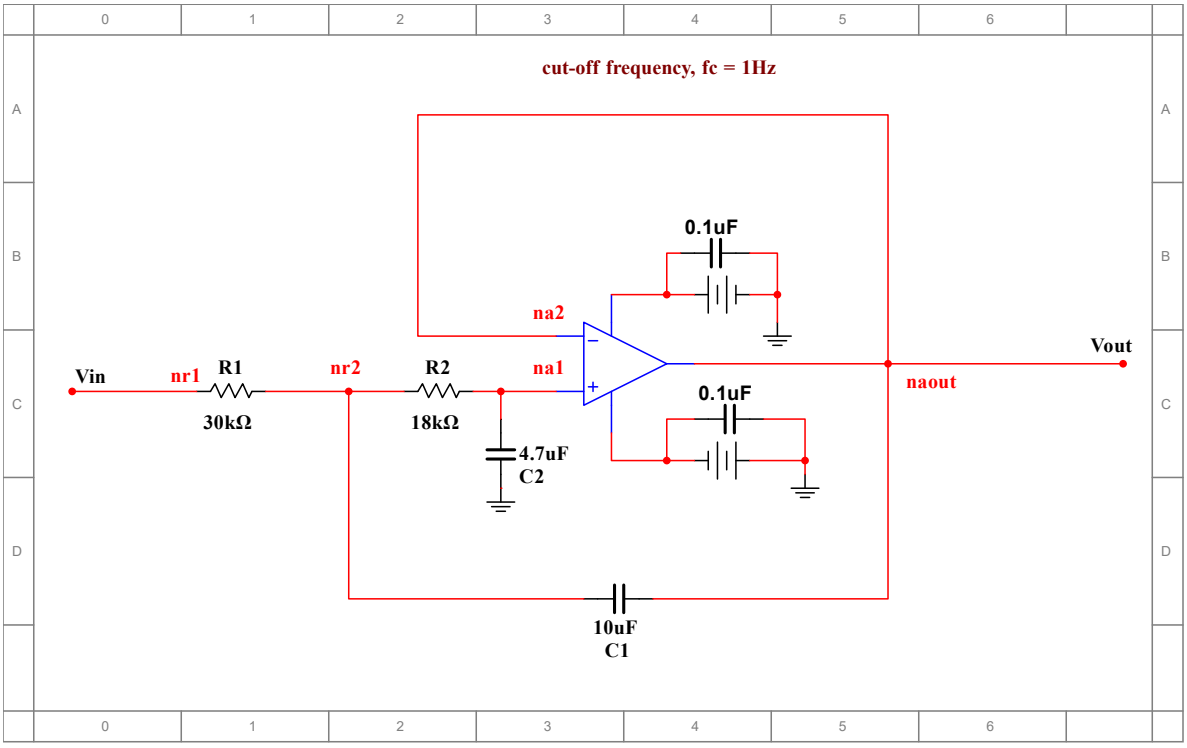

Figure 20: Sallen-Key Filter

The transfer function of above design can be written as below,

$$\frac{V\text{out}}{V\text{in}} = \frac{\frac{1}{R_1\,C_1\,R_2\,C_2}}{s^2 + s(\frac{1}{R_2\,C_1} + \frac{1}{R_1\,C_1}) + \frac{1}{R_1\,C_1\,R_2\,C_2}} \tag{15}$$

In order to calculate the values of resistors and capacitors using the cut-off frequency, fc = 1Hz and quality factor, Q = $1/\sqrt{2}$, we used the following formulas,

$$fc = \frac{1}{2\pi\,\sqrt{R_1\,C_1\,R_2\,C_2}} \tag{16}$$

$$Q = \frac{1}{2\,\zeta} \tag{17}$$

where ζ is the damping ratio.

The values of capacitance C_1 and C_2 are kept such that

$$\frac{C_2}{C_1} \leq \zeta^2 \tag{18}$$

$$\frac{C_1}{C_2} \geq 4\,Q^2 \tag{19}$$

Considering the above formulas we calculated the values of R_1=30kΩ, R_2=18kΩ, $C_1 = 10\mu$F and $C_2 = 4.7\mu$F.

The noise of the sallen-key was also studied using the SR785 spectrum analyzer. The noise is very much dominated by the noise of the OP27 itself.

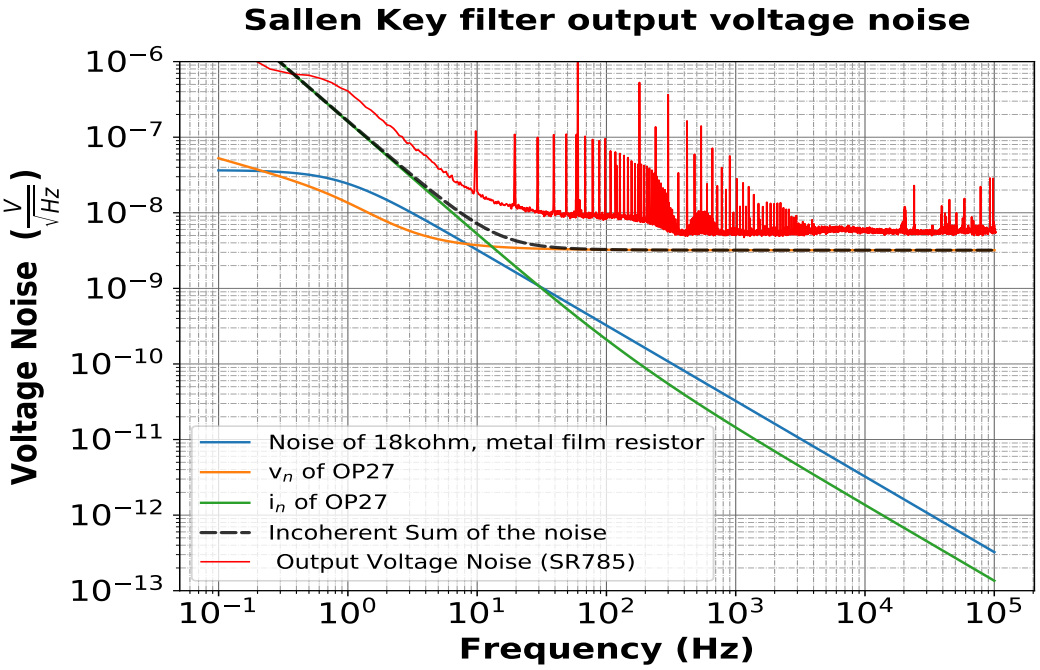

Figure 21: Noise across Sallen-Key

5.6 Voltage Regulator

The 15V supply is very noisy when taken from voltage supplies available in lab. So a voltage regulator circuit was made in order to nullify the incoming unwanted noise. The regulators that can be used for this purpose are LM317,LM337, LM7915 and LM7815. The circuit below shows the configuration of regulators. We provided a 18V(+/-) input to get a regulated output of 15V(+/-). For these voltage regulators we keep a cut-off of 3V between the input and output. These voltage regulators were used to provide the bias to the OpAmps used in TIA, Sallen Key, differential amplifier and whitening filter.

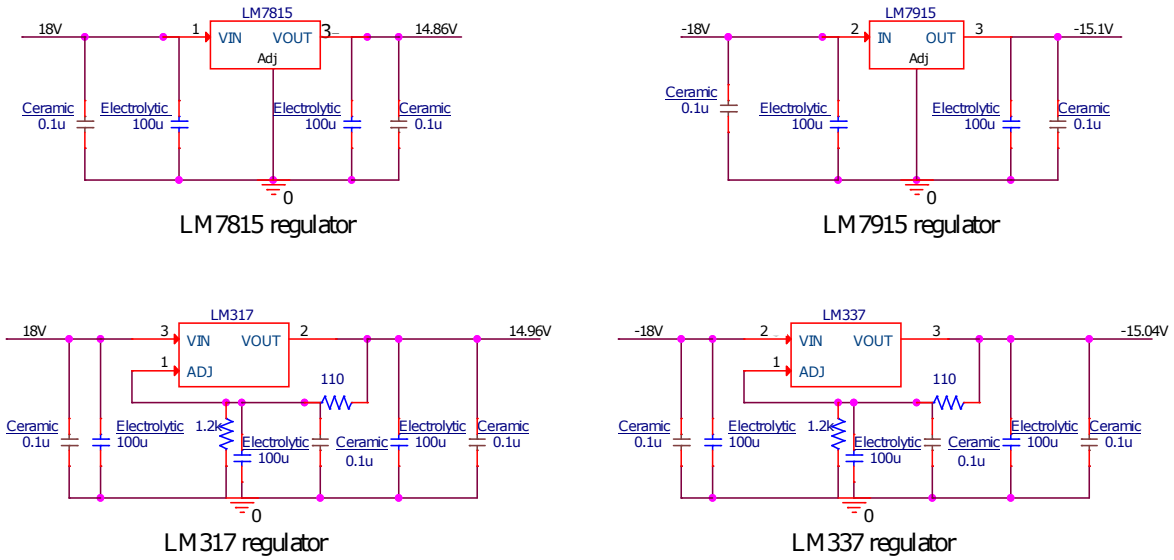

Figure 22: Voltage Regulators

For the LM317, a positive voltage regulator the below formula was used to decide the value of resistors. This helped us in adjusting the output to 14.96 V.

$$Vout = 1.25\,(1 + \frac{R_2}{R_1}) \tag{20}$$

We chose the values of R_1=110 Ω and R_2=1.2 kΩ.

Similarly, in case of LM337, a negative voltage regulator, we used the below formula to select the values of the resistors.

$$Vout = -\,1.25\,(1 + \frac{R_2}{R_1}) \tag{21}$$

We chose the values of R_1=110 Ω and R_2=1.2 kΩ to get the desired output of -15.04 V.

We measured the noise across each regulator circuit in order to know which regulator will be least noisy and appropriate for our experiment. At 10 Hz, we observed voltage noise to be 0.3 $\mu A/\sqrt{Hz}$ for LM317, 0.6 $\mu A/\sqrt{Hz}$ for LM337, 0.7 $\mu A/\sqrt{Hz}$ for 7815 and 2 $\mu A/\sqrt{Hz}$ for LM7915. We observed that LM317 will be good as a positive voltage regulator and LM337 will be good as a negative voltage regulator as they both have least noise.

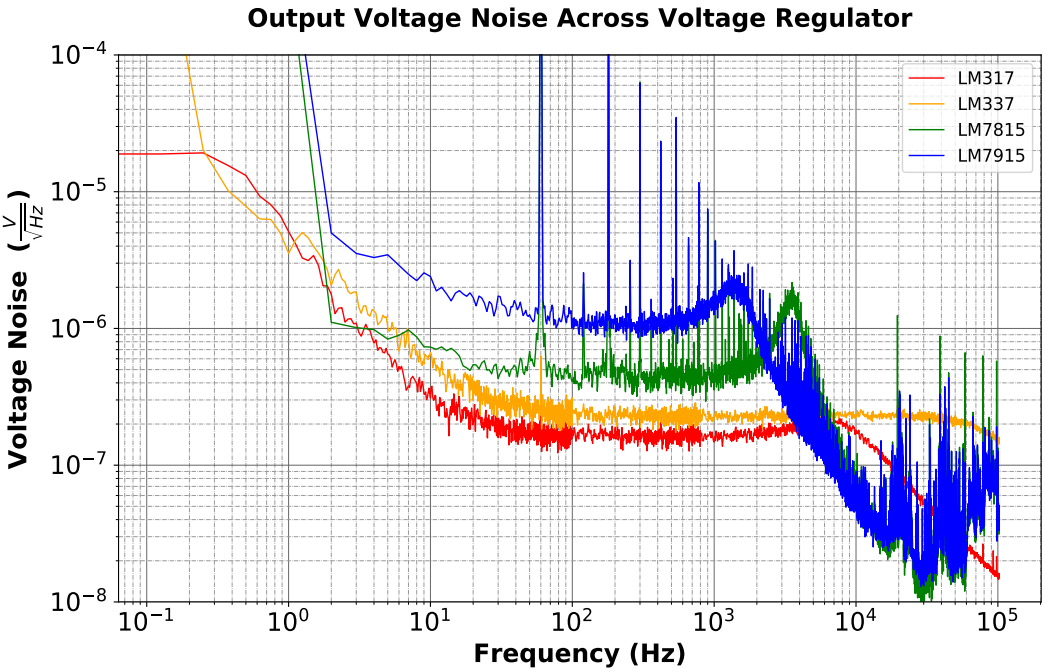

Figure 23: Comparison between different regulator's noise

5.7 Dark Current Measurement of Photodiodes

Even in the absence of any incident laser power, the photodiode still produces some signal current on being provided a bias voltage. We analyzed the dark current for both extended-InGaAs and InAsSb photodiodes.

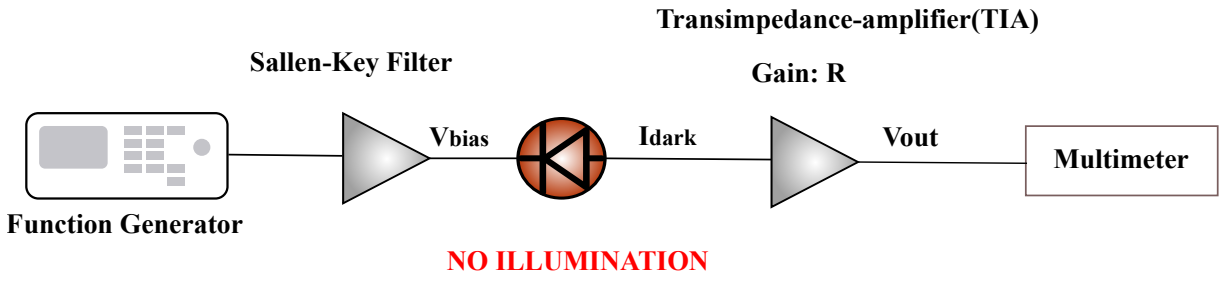

Figure 24: Setup for Dark Current Measurement

The TIA(with gain R) converts dark current into voltage. So, in order to obtain the dark current we use the formula,

$$I\text{dark} = \frac{V\text{out}}{R} \tag{22}$$

5.7.1 Extended-InGaAs Photodiodes

There were two photodiodes of same material, namely X8905 and X8906. Measurements were taken for both of them to know which one is better. The maximum reverse bias voltage that can be applied to the extended-InGaAs is 1V. We applied a range of voltages and observed the dark current for each bias voltage.

For X8905 we observed the dark current to be -19 μA at a bias voltage of 1 V. Whereas, for X8906 the dark current was observed to be -6 μA.

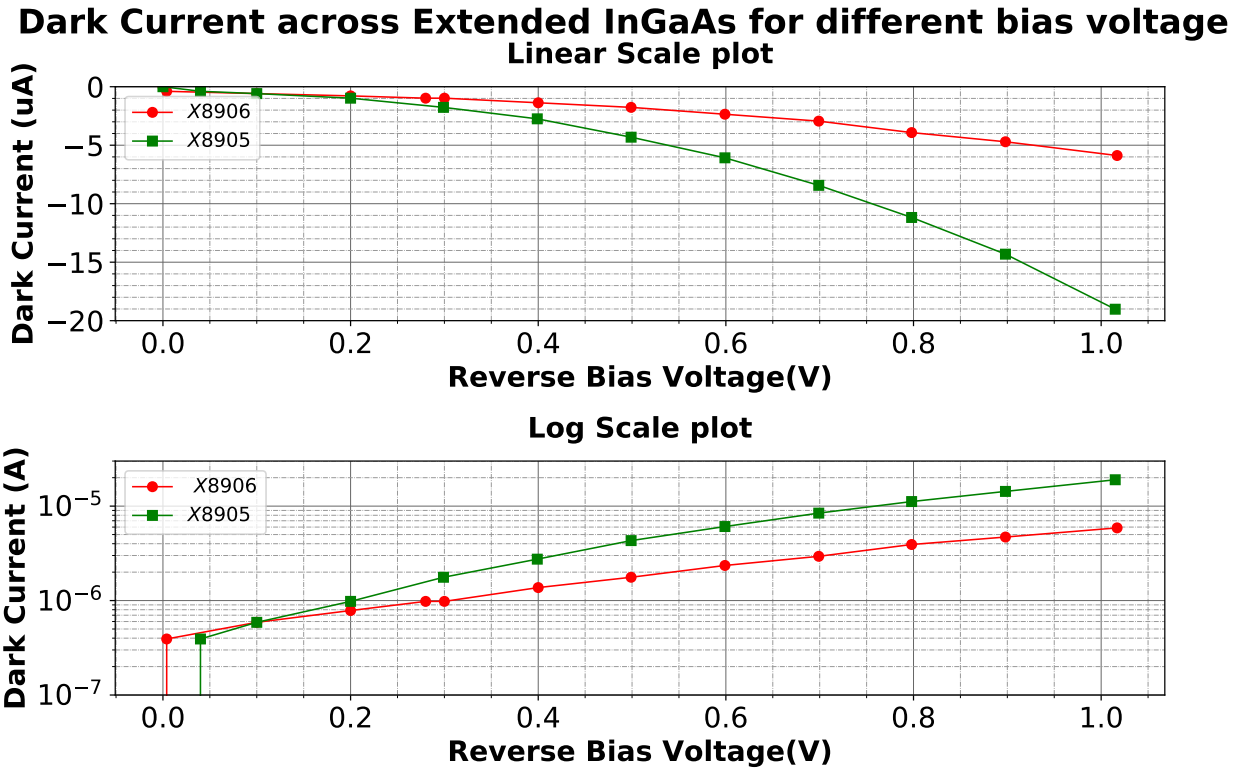

Figure 25: Dark Current of Extended-InGaAs

The Extended-InGaAs are 2mm in diameter. Dark current density was calculated by dividing dark current with the area of PD. Again it was observed that X8906 has least dark current density. Hence it is better as compared to X8905.

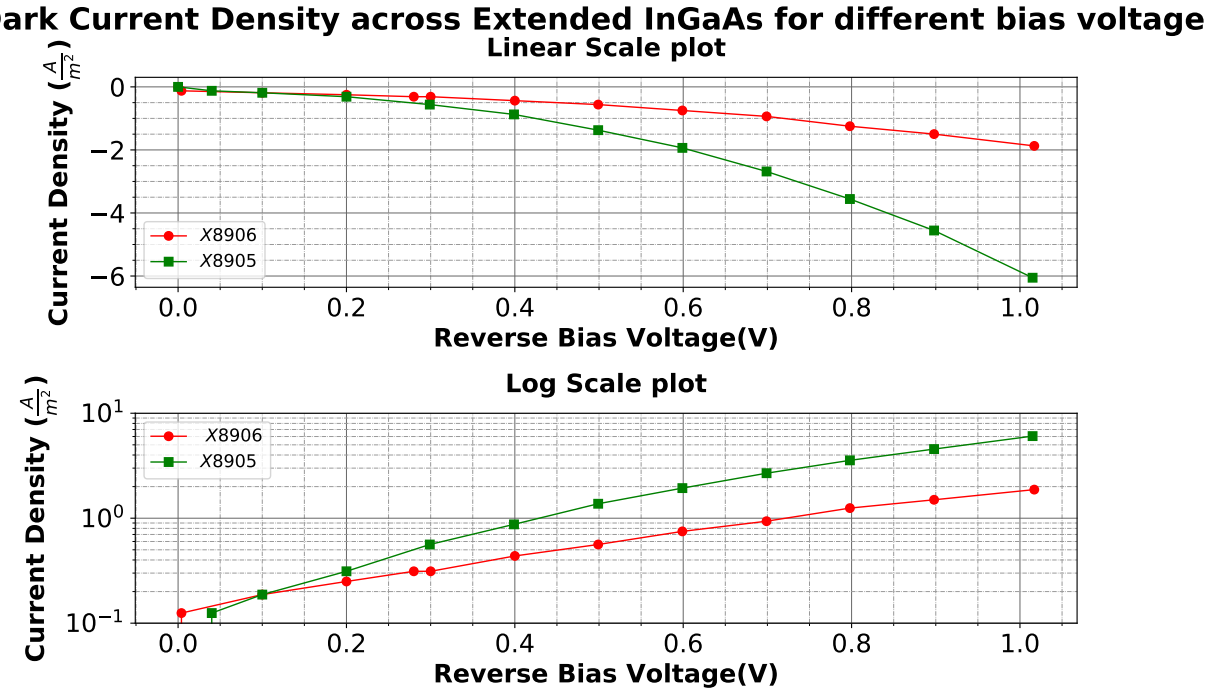

Figure 26: Dark Current Density of Extended-InGaAs

5.7.2 InAsSb Photodiodes

The Sb3513_A2 photodiodes have 3 photodiodes of different areas, $(500\mu\text{m})^2$, $(750\mu\text{m})^2$, $(1000\mu\text{m})^2$, on the same substrate. The maximum reverse bias voltage that could be applied to this photodiode is 0.3 V.

We observed that the photodiode with area $(500\mu\text{m})^2$ produces the maximum dark current. At the maximum bias of 0.3 V, the $(500\mu\text{m})^2$ produces a dark current of 0.75 mA.

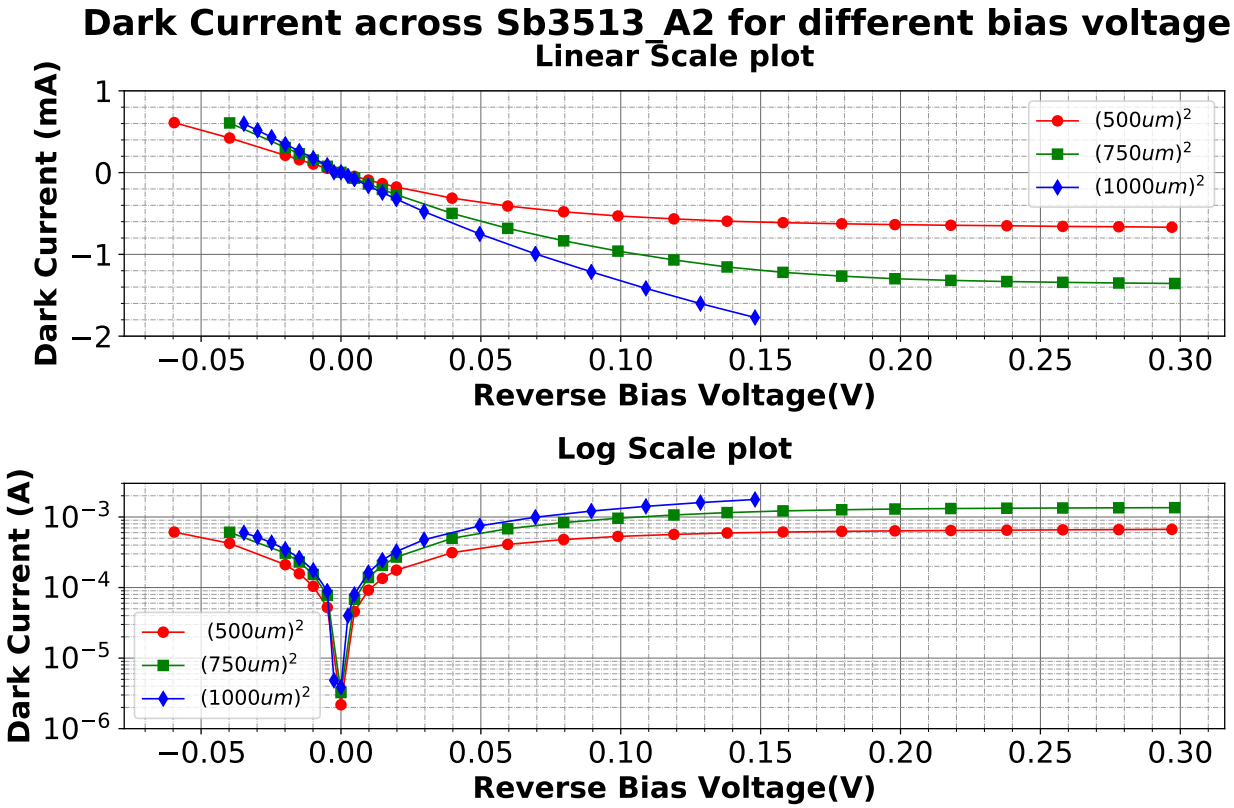

Figure 27: Dark Current of InAsSb

We can calculate the current density by dividing the dark current with respective area. We observed that photodiode with area $(500\mu\text{m})^2$ has the least dark current density. Hence $(500\mu\text{m})^2$ is better as compared to other areas taken into account.

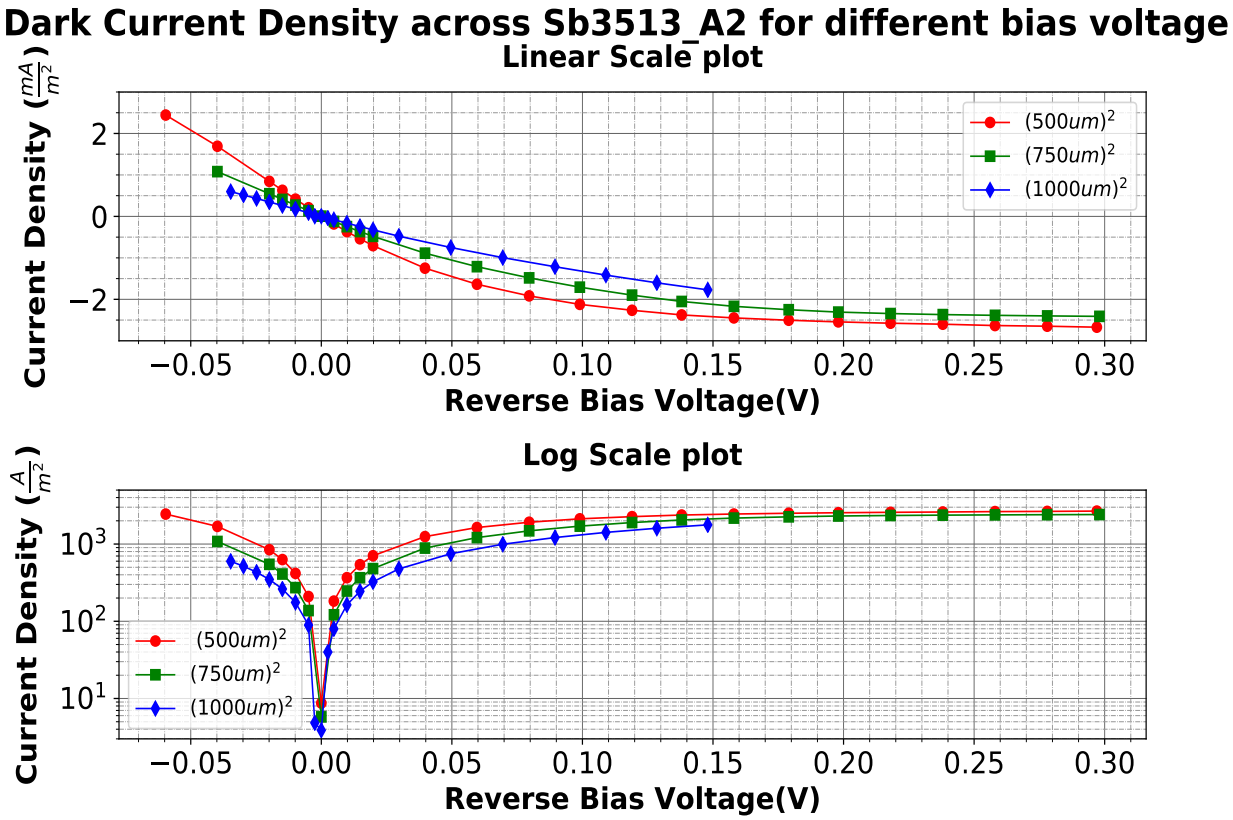

Figure 28: Dark Current Density of InAsSb

5.7.3 Comparison between photodiodes

When we compared the dark current produced from ex-InGaAs and InAsSb, we found that ex-InGaAs(X8906) produced the least dark current out of all the other PD.

At maximum bias of 1V for ex-InGaAs, the dark current was observed to be $6\mu A$. At maximum bias of 0.3 V for InAsSb, the dark current was observed to be 0.7 mA.

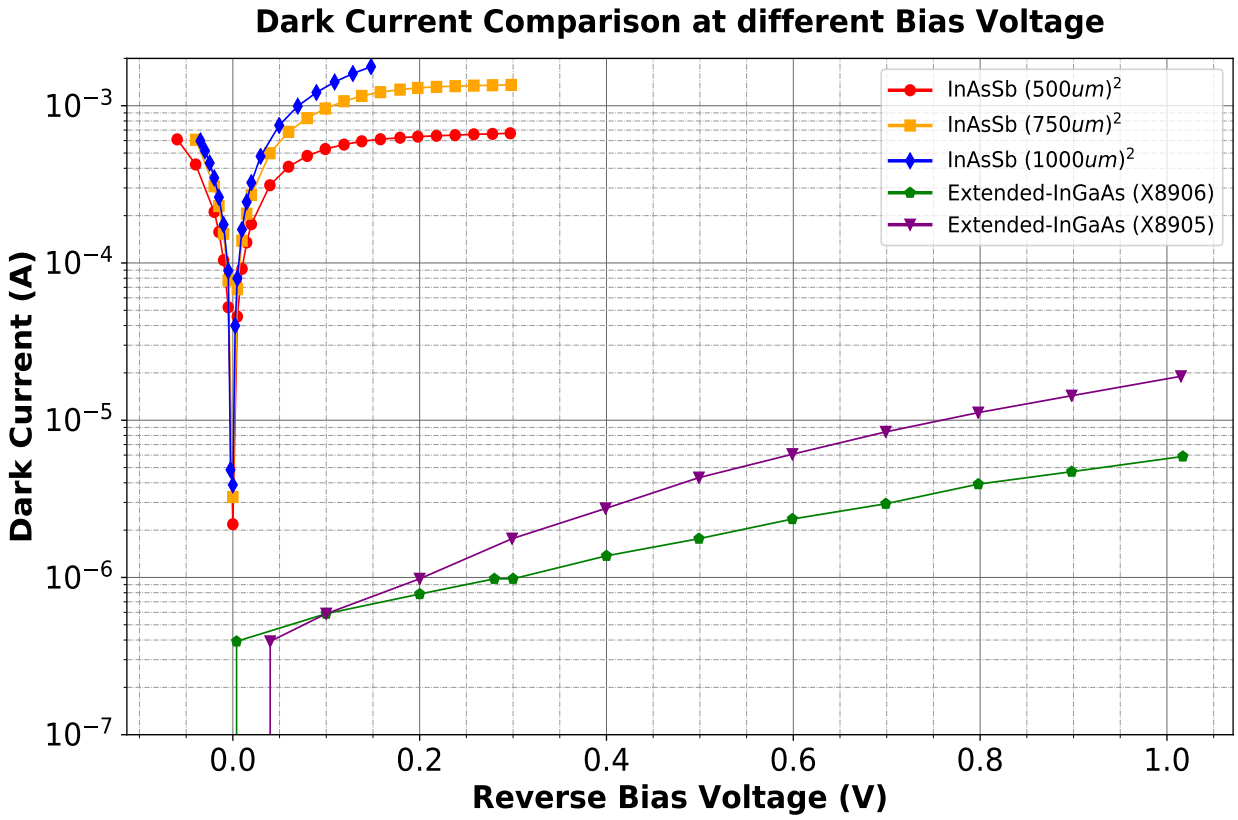

Figure 29: Dark Current Comparison

5.8 Dark Noise Measurement of Photodiodes

Even in the absence of any incident power the dark current that is produced adds to the noise of the circuit in the form of dark noise. We observed it using the SR785 spectrum analyzer.

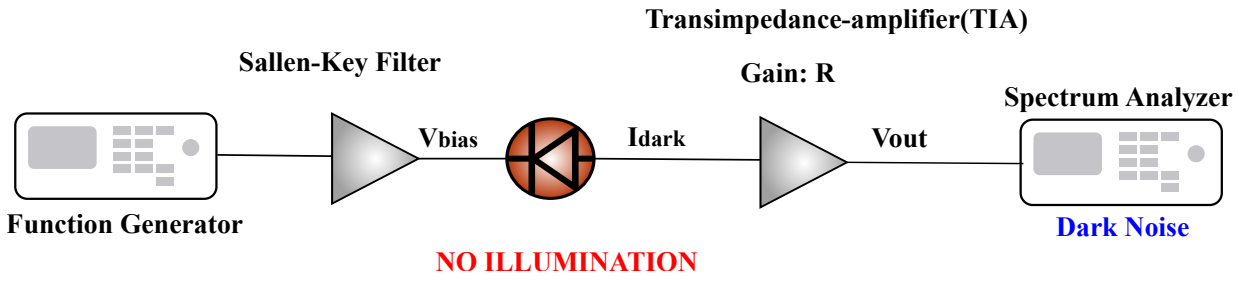

Figure 30: Setup for Dark Noise Measurement

5.8.1 Extended-InGaAs Photodiodes

We had observed that X8906 produced less dark current as compared to X8905. We studied the dark noise for different bias voltages. The results were as expected. X8906 produced less dark noise as compared to X8905, for same bias voltage applied.

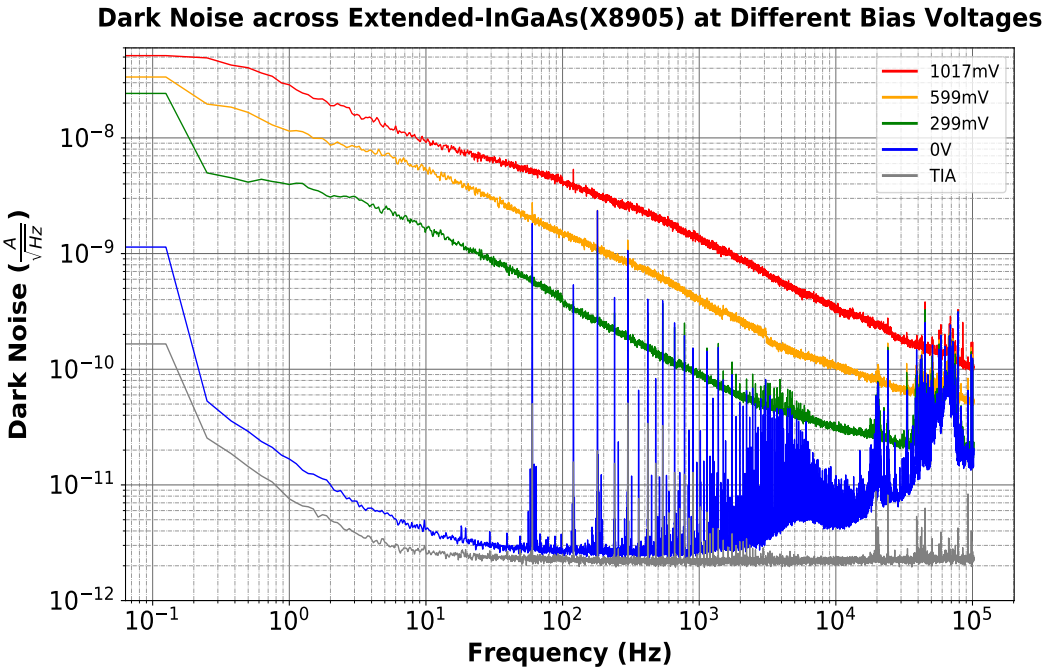

Figure 31: Dark Noise of Extended-InGaAs(X8905)

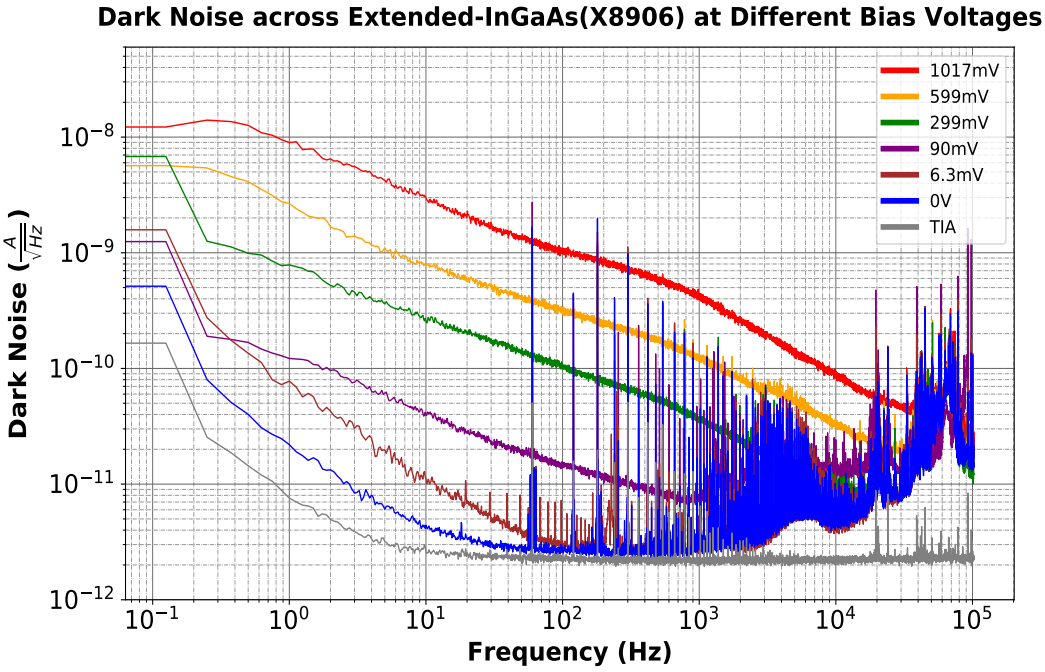

Figure 32: Dark Noise of Extended-InGaAs(X8906)

It was observed that the dark noise decreases with decrease in bias voltage. At around 0V, the setup gets limited by the noise of the transimpedance amplifier. Hence, it won't be good to provide a bias of 0V.

We observed the dark noise produced at maximum bias of 1 V to be, 10 nA/$\sqrt{\text{Hz}}$ and 3 nA/$\sqrt{\text{Hz}}$ from X8905 and X8906 respectively, at 10 Hz. The dark noise from X8906 was less in compared to X8905.

5.8.2 InAsSb Photodiodes

The dark noise was observed for all three areas on the substrate. It was observed that the dark noise decreases with decrease in bias voltage, for each of the three areas.

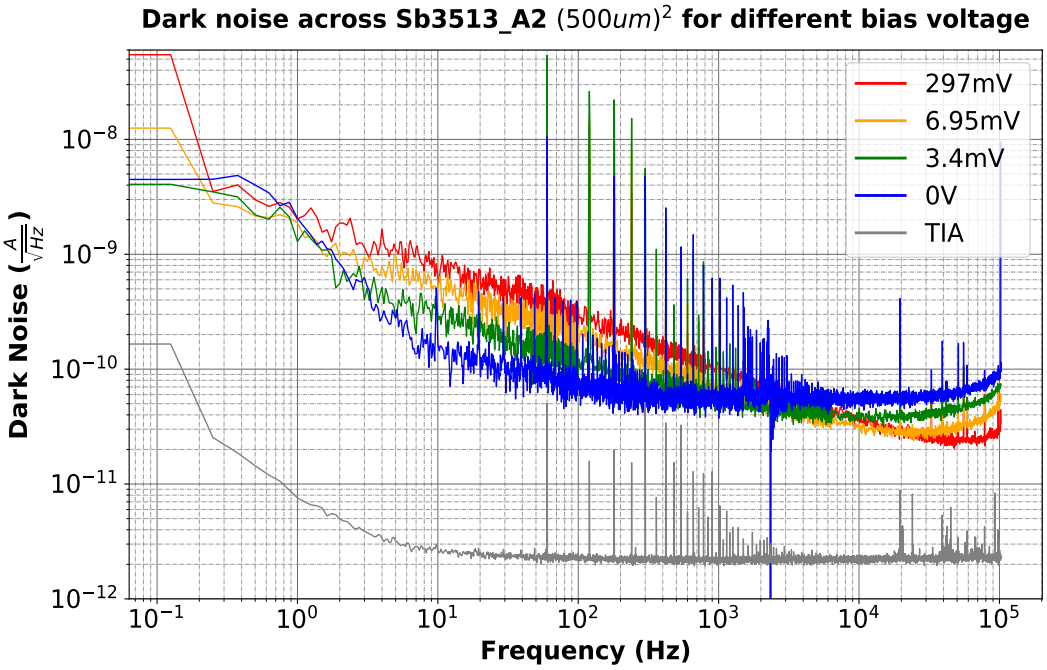

Figure 33: Dark Noise of InGaAs $(500\mu m)^2$

The dark noise produced from $(500\mu m)^2$ at maximum bias of 297 mV was 1 nA/$\sqrt{\text{Hz}}$ at 10 Hz. At a bias of 0 V, the noise observed was 0.1 nA/$\sqrt{\text{Hz}}$ at 10 Hz.

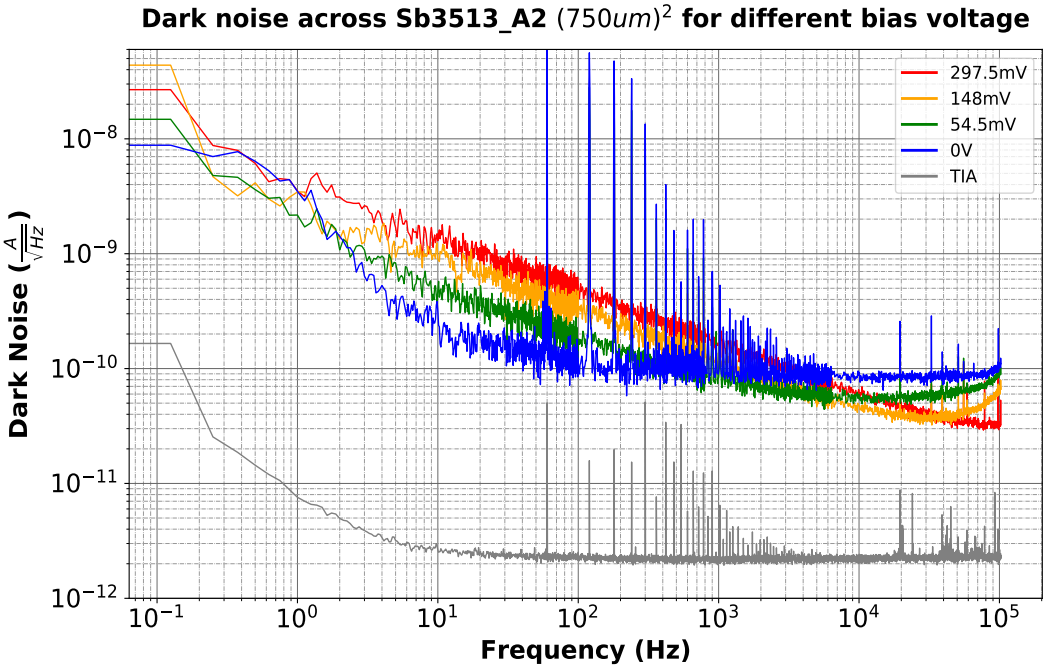

Figure 34: Dark Noise of InGaAs $(750\mu m)^2$

The dark noise produced from $(750\mu m)^2$ at maximum bias of 297.5 mV was 1.5 nA/$\sqrt{\text{Hz}}$ at 10 Hz. At a bias of 0 V, the noise observed was 0.2 nA/$\sqrt{\text{Hz}}$ at 10 Hz.

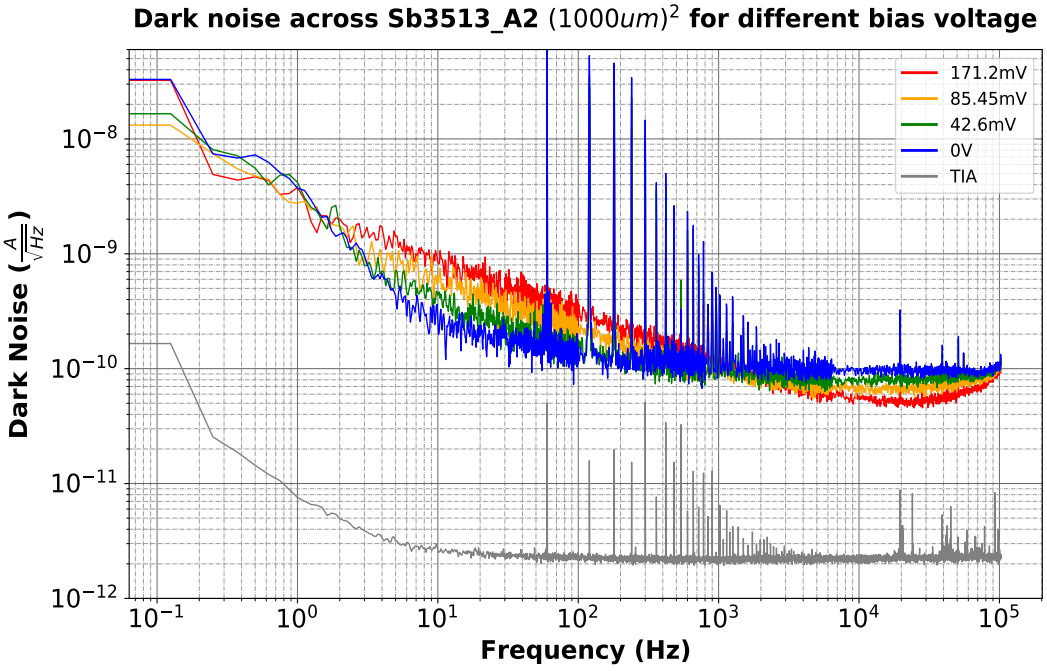

Figure 35: Dark Noise of InGaAs $(1000\mu m)^2$

The dark noise produced from $(1000\mu m)^2$ at bias of 171.2 mV was 1 nA/$\sqrt{\text{Hz}}$ at 10 Hz. At a bias of 0 V, the noise observed was 0.3 nA/$\sqrt{\text{Hz}}$ at 10 Hz.

5.8.3 Comparison between photodiodes

We observed that ex-InGaAS, X906 and InAsSb with area $(500\mu\text{m})^2$, perform better as compared to the ones made of same material. Therefore we compared these two and found that, at room temperature ex-InGaAs produces less dark noise at maximum bias voltage.

At a frequency of 10Hz, the noise observed to be 0.1 $\text{nA}/\sqrt{\text{Hz}}$ from InAsSb with area $(500\mu\text{m})^2$, at maximum bias of 297 mV. At 10Hz, the noise from ex-InGaAS was 3 $\text{nA}/\sqrt{\text{Hz}}$, at maximum bias of 1 V.

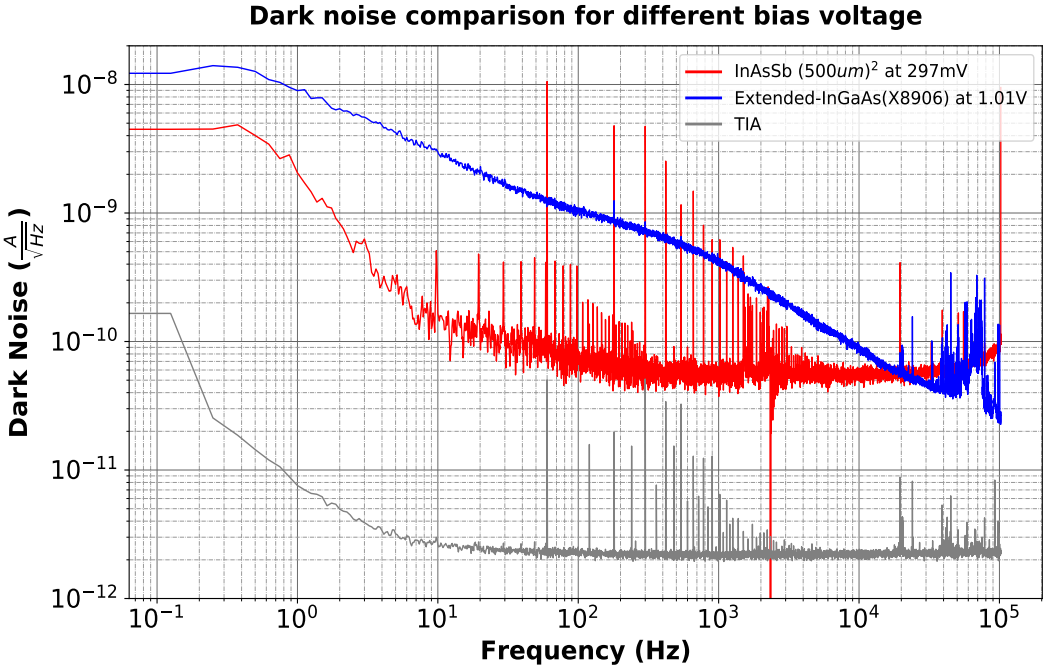

Figure 36: Dark Noise Comparison at Maximum Bias

5.9 1/f noise Measurement of Photodiodes

$1/f$ noise or flicker noise is the noise that dominates at low frequencies. We observe the dark noise for different bias voltages at 10Hz for both the photodiodes.

5.9.3 Extended-InGaAs Photodiodes

X8906 has less $1/f$ noise as compared to X8905. At maximum bias of 1 V, 9 nA/$\sqrt{\text{Hz}}$ and 2.5 nA/$\sqrt{\text{Hz}}$ for X8905 and X8906 respectively. The 1/f noise was observed to increase with increase in bias voltage.

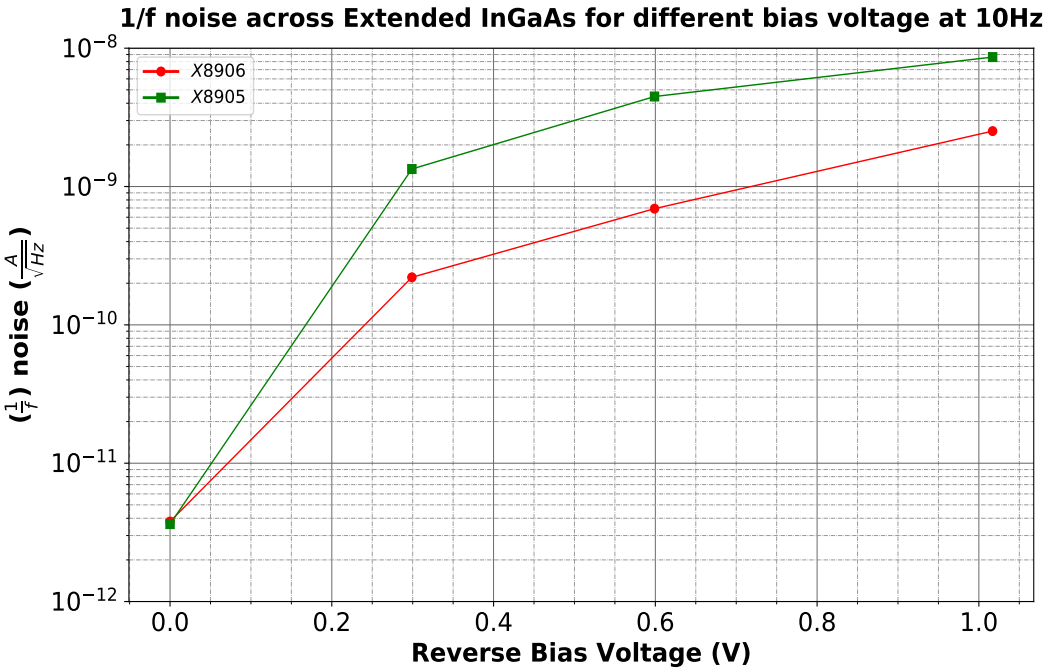

Figure 37: 1/f noise of Extended-InGaAs

5.9.2 InAsSb Photodiodes

PD with area $(500\mu\text{m})^2$ was obsvered to have least 1/f noise at maximum bias voltage of 0.3 V. The $1/f$ noise was observed to be 0.7 nA/$\sqrt{\text{Hz}}$ and 0.93 nA/$\sqrt{\text{Hz}}$ from $(500\mu\text{m})^2$ and $(750\mu\text{m})^2$ respectively, at a maximum bias of 0.3 V. It was observed that the $1/f$ noise increases with increase in area at higher bias voltages and increases with decrease in area at lower bias voltages.

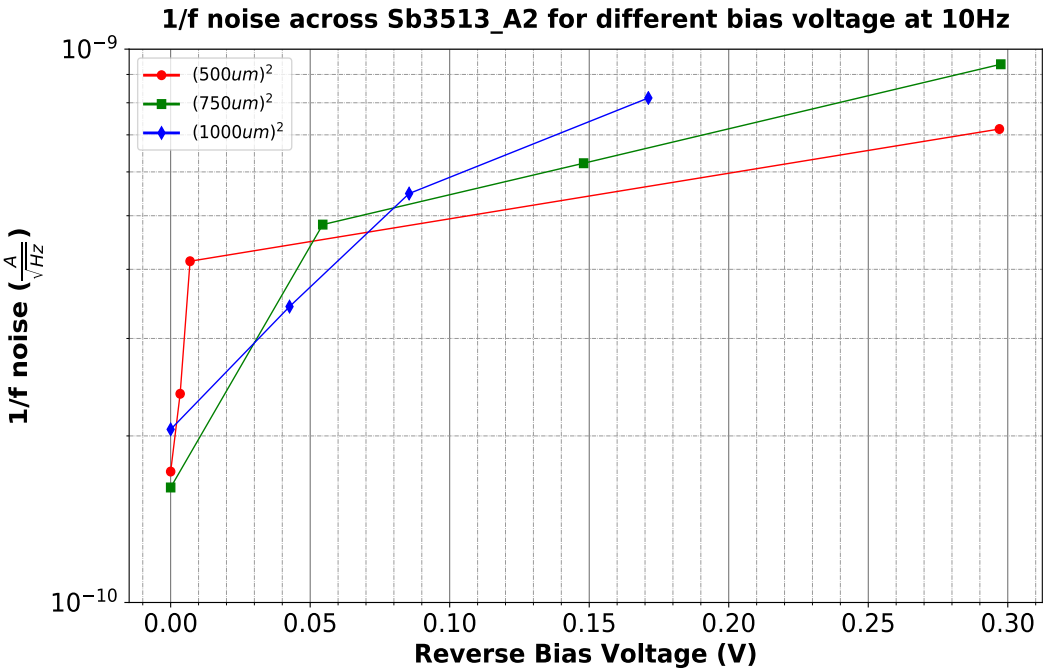

Figure 38: $1/f$ noise of InAsSb

5.9.3 Comparison between photodiodes

It was observed that ex-InGaAs photodiodes have less $1/f$ noise as compared to InGaAs PD at 10 Hz.

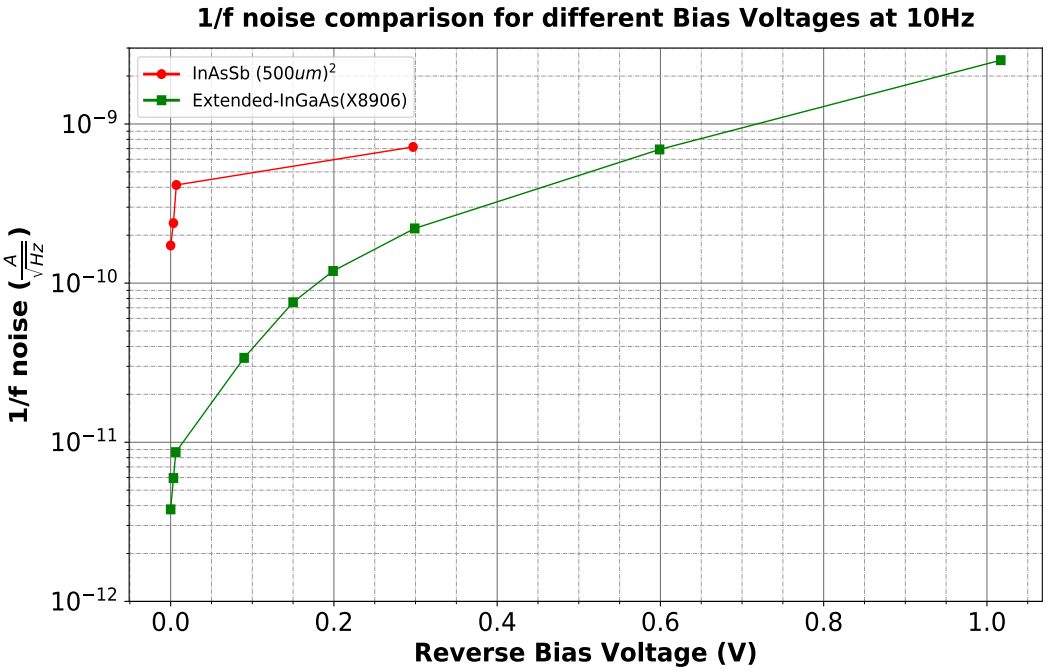

Figure 39: $1/f$ Noise comparison

5.10 Quantum Efficiency(Q.E.) Measurement of Photodiodes

When the laser power is incident on the photodiode, the photodiode produces some photocurrent on applied a bias voltage. But not all power incident is used in producing the photocurrent. Some amount of incident power is reflected. If we consider that all of the incident power was utilized by the PD, we can know about the external quantum efficiency. Taking into account the reflectivity and subtracting it, we can know about the internal quantum efficiency.

For this experiment the incident power was 0.80 mW. It was checked using the ophir RM9 power meter.

In the below setup, Vbias is the bias voltage applied to the PD, Pin is the incident laser power on the PD and Prefl is the reflected power, Iph is the photocurrent produced. Using the TIA, the current is converted into voltage.

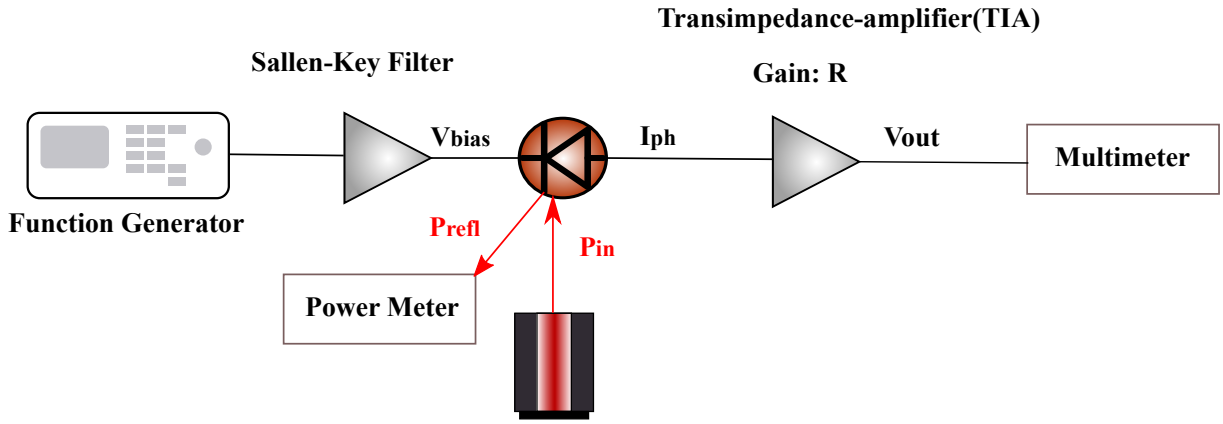

Figure 40: Setup for Quantum Efficiency Measurement

The External and Internal Q.E were calculated by using the following formula and from equation 3 and 4,

$$E.Q.E. = \frac{I\mathrm{ph}\,/\,e}{P\mathrm{in}/\,h\,\nu} \tag{23}$$

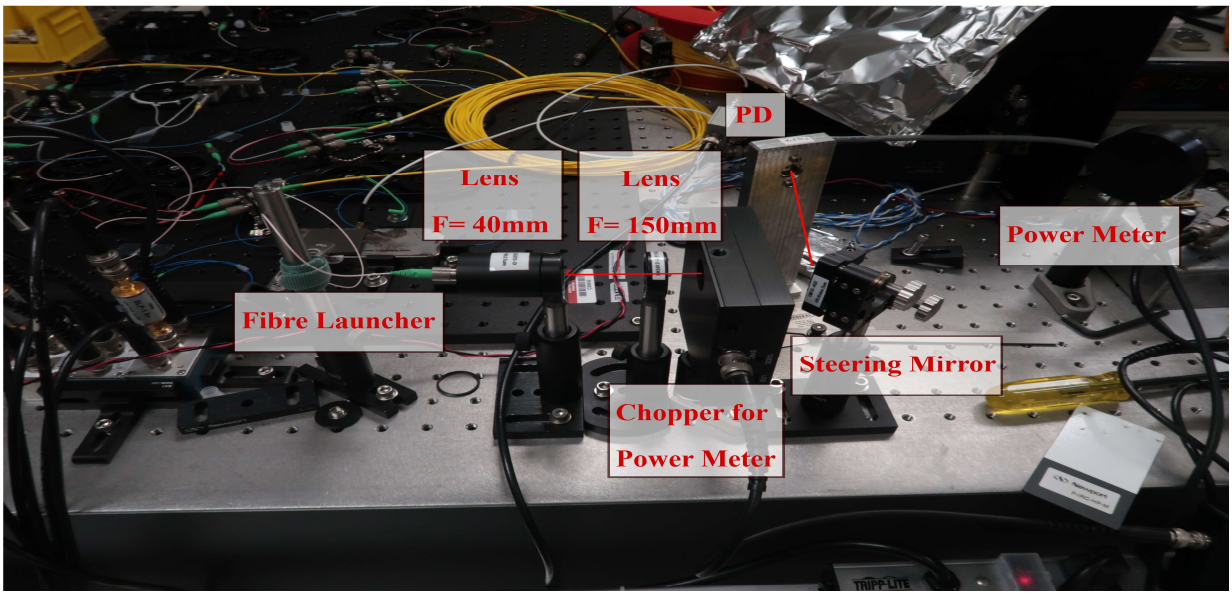

Figure 41: The setup on an optical bench

5.10.1 Extended-InGaAs Photodiodes

We observed that ex-InGaAs(X8906) performed well in comparison to other photodiodes, at room temperature. So, we tested the Q.E of this PD at room temperature. At maximum reverse bias of 1 V, the external Q.E. was observed to be 77.4% and the internal Q.E. was calculated to be 83.8%, taking into account the reflectivity of 0.6 μW at 17deg.

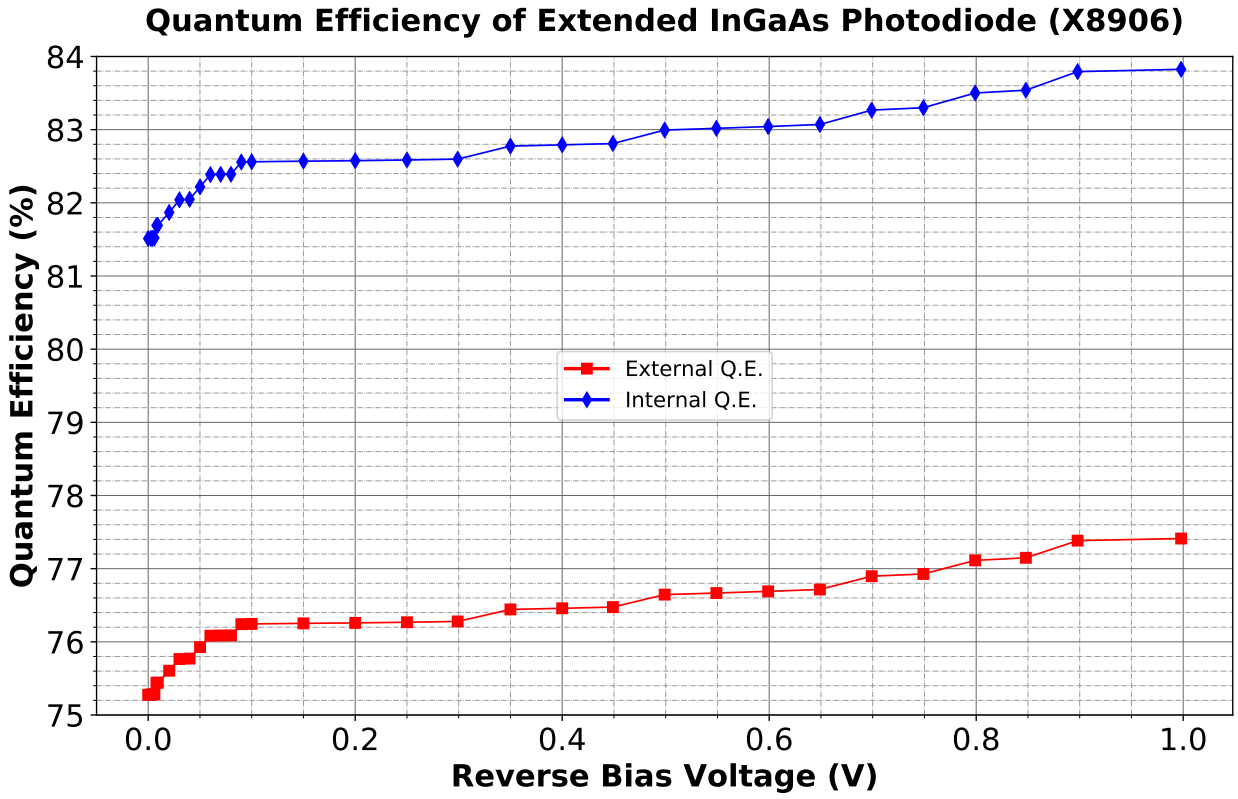

Figure 42: Quantum Efficiency of ex-InGaAs(X8906)

6 Conclusion

The TIA with low noise was designed to characterize the PD which are sensitive to 2 μm of laser wavelength. The dark noise, dark current and flicker noise of ex-InGaAs and JPL InAsSb was observed and compared at room temperature. We observed that at room temperature the ex-InGaAs(X8906) prodcuced the least dark current, dark noise and $1/f$ noise. Hence we stuided the external and internal Q.E. of ex-InGaAs PD, at room temperature and found it to be 77.4% and 83.8% respectively, at the maximum applied bias.

7 Future Work

We can design a whitening filter that will be appropriate to use with the differential circuit described above. We can test the quantum efficiency of JPL InAsSb photodiodes at room temperature. We can study the quantum efficiency as the function of bias voltage, of the photodiode and know how are the related. We can also test the quantum efficiency, dark current and dark noise of the photodiodes at lower temperature, in a cryotstat. We can test other materials of photodiodes that are sensitive to 2 μm of laser wavelength, for example Mercury Cadmium Telluride(HgCdTe).

References

[1] *Advanced LIGO*. arXiv:1411.4547(2014)

[2] Peter Csatorday, *LIGO Photodiode Characterization and Measurement of the Prestabilized Laser Intensity Noise*. Massachusetts Institute of Technology, Dept. of Physics(1999)

[3] Adhikari, Rana X, et. al, *LIGO Voyager Upgrade: Design Concept*. LIGO Scientific Collaboration, LIGO-T1400226-v9 (2014)

[4] Koji Arai, *DT5: Design of whitening filters for DT5*. National Astronomical Observatory, TAMA project(February 21, 2001)

[5] J. Briggs, K. Strain, S. Hild, B. Barr, A. Spencer and A. Bell, *Dark Noise, Dark Current, Linearity and Quantum Efficiency at 1550 nm of InGaAs and Extended InGaAs Photodiodes*. (July 27, 2018)